Revisiting Dolomitization in the Isla De Mona Isolated Carbonate Platform: Marine, Mixing, Reflux, or Biogenic?

By

Paula D. Richter

B.S., University of Wisconsin-Oshkosh, 2011

Submitted to the graduate degree program in Geology and the Graduate Faculty of the University of Kansas in partial fulfillment of the requirements for the degree of Master of Science.

_____

Chair: Luis González

_____

Co-Chair: Robert Goldstein

_____

Jennifer Roberts

Date Defended: November 30th 2016

The Thesis Committee for Paula Richter
certifies that this is the approved version of the following thesis:

Revisiting Dolomitization in the Isla de Mona Isolated Carbonate Platform: Marine, Mixing, Reflux, or Biogenic?

_____
Chair Luis González

_____
Co-chair Robert Goldstein

Date approved: November 30th 2016

Abstract:

Predicting the origin of dolomite is critical to understanding porosity and permeability in conventional oil and gas reservoirs. Studies evaluating the mechanism for dolomitization can be applied to those reservoirs as models for predicting porosity distribution. This study provides a test of the mixing-zone dolomitization model and explores alternative explanations in an area where geochemical data suggest a mixing-zone origin.

The purpose of this study is to determine the origin of dolomite in Miocene and Pliocene strata on Isla de Mona, a small island off the western coast of Puerto Rico. The island is composed of two formations; the upper is the Lirio Limestone and the lower is the partially dolomitized Isla de Mona Limestone. Given the geologic setting of Isla de Mona, four dolomitization models were considered plausible and consistent with published stable isotope data—marine, mixing zone, reflux, or biogenic.

The petrography and cathodoluminescence show at least two recrystallized dolomite phases. Later luminescent phases do not show signs of recrystallization. Fluid inclusion data range from 35 to 63 ppt salinity. Isotope data show a linear trend between fresh and evaporated seawater end members. These results exclude a marine or biogenic origin for most of the dolomite because the salinity values are higher than expected for those models. Mixing of fresh and evaporated marine fluids could not be ruled out, but petrography and fluid inclusion ranges make this explanation unlikely. The most likely explanation for the isotope data is a physical mixture between: dolomite that was recrystallized in fresh water; and a non-recrystallized dolomite, which formed in seawater and evaporated seawater. When the island was exposed, fresh water recrystallized the

early dolomite phases. When sea level was high, evaporation and reflux occurred, which led to precipitation of later dolomite phases.

Acknowledgements:

I would first and foremost like to thank my committee members Luis González, Robert Goldstein, and Jennifer Roberts, for their guidance, and all their help during the course of this research. I would also like to thank the University of Kansas Department of Geology, and the KPESIL lab. Additional funding was provided by Chevron and Encana Energy. This research would also not have been possible without the samples provided by Alejandra Rodríguez-Delgado, and her previous work, which this study is built upon. I would like to thank Dr. Dan Lehrmann, whose enthusiasm inspired my interest in carbonates, and for giving me the tools and opportunities I needed to succeed at school and professionally. I thank Austin Shock for his advice, help with illustrator, and his motivational pep talks. Finally, I would like to thank Alicia Rosales, for not only being my first friend at KU, but a continued close friend, and for spending time working on her thesis with me.

Table of Contents

Abstract: iii
Acknowledgements: iv
Introduction: 1
Geologic Setting: 3
Methods: 7
Results: 9
General aspects of petrography: 9
Paragenesis: 10
Dolomite distribution: 14
Fluid inclusions: 15
Stable Isotopes: 16
Discussion: 17
Conclusions: 25

List of figures

Figure 1: Representative cross sections of major dolomitization models..... 31
Figure 2: Graph of saturation index versus percent seawater. 32
Figure 3: Location map of Isla de Mona and the Mona Passage. 32
Figure 4: List of facies and interpreted depositional environments..... 33
Figure 5: Map showing the distribution of environments on Isla de Mona. 34
Figure 6: Cross section showing distribution of the dolomite along the cliffs of IM. 35
Figure 7: Geologic map of Isla de Mona showing locations of measured sections..... 36
Figure 8: Stratigraphic columns for the measured sections analyzed. 37
Figure 9: List and relative timing of paragenetic events..... 38
Figure 10: Transmitted light and CL image from sample PE-2..... 38
Figure 11: Transmitted light and CL image of sample CGS-4..... 39
Figure 12: Transmitted light and CL image of a sample from UVE-3. 39
Figure 13: Transmitted light and CL image of a sample from UVE-3. 40
Figure 14: Transmitted light and CL image of a sample from UVE-1. 40
Figure 15: Graph of percent dolomite versus percent extant porosity. 41
Figure 16: Photomicrographs of fluid inclusions..... 41
Figure 17: Histogram of fluid inclusion data. 42
Figure 18: Crossplot of stable isotope data. 42
Figure 19: Graph of average fluid inclusion salinity versus $\delta\ ^{13}C$..... 43
Figure 20: Graph of average salinity versus $\delta\ ^{18}O$..... 43

Introduction:

Dolomitization is thermodynamically feasible at the Earth's surface, but at low temperature the process is typically hindered by kinetic factors (i.e. reactions are too slow). Kinetic factors can be overcome and dolomite precipitation facilitated by several processes that could lead to dilution of supersaturated fluids, increased fluid Mg/Ca, or increased fluid CO_3/Ca (Morrow, 1982a). Numerous hypotheses have been proposed to explain dolomitization in different settings and they include the following models (Figure 1): 1) reflux/sabkha; 2) burial compaction; 3) hydrothermal; 4) mixing zone (Dorag) (Morrow, 1982b); and 5) biogenic (Krause et al., 2012).

The mixing zone model, which suggests that dolomitization occurs in the zone of mixing between marine and fresh waters, is the focus of this study. In some cases, the mixture of calcite-saturated marine and fresh waters can produce a fluid that is undersaturated with respect to calcite and saturated with respect to dolomite (Figure 2; e.g. Badiozamani, 1973; Land, 1973; Hanshaw et al., 1971). In this setting, the flux of marine waters into the existing fresh waters can provide a source of magnesium ions (Gasworth et al., 2007). Because this type of dolomite could form over a range of fluid compositions between fresh and marine end-members, dolostones and dolomite cements formed in this way can have highly variable but predictable stable isotopic, and trace elemental compositions. As evidence of pervasive dolomitization in mixing zones is questionable, many researchers have argued against this mechanism for producing pervasive dolomite (Smart et al., 1988; Price and Herman, 1991; Maliva et al., 2001; Melim et al., 2004; Csoma et al., 2004; 2006; Hardie, 1987; Machel and Mountjoy, 1986; Machel, 2004; Melim et al., 2002). Other researchers have challenged previous

interpretations of mixing-zone dolomite on the basis of evidence for partial resetting of dolomite geochemistry in fresh or high-temperature fluids (Land, 1991; Machel and Burton, 1994; Luczaj, 2006). Recently, mixing of slightly evaporated marine and fresh waters has been hypothesized as a method for producing pervasive dolomite (Li et al., 2013; Meyers et al., 1997). Both of these studies focused on Miocene dolostones in Spain. Meyers et al. hypothesized that the analyzed dolomite formed when evaporated brines created during sea level falls mixed with fresh water during sea level rises. The model hypothesized by Li (2013) involved ascending fresh water recharge, which mixed with evaporated brines.

Isla de Mona (IM), an isolated carbonate platform in the Caribbean, originally was hypothesized to have been dolomitized by mixing-zone processes (González et al., 1997) based on stable isotope values and dolomite characteristics. The stable isotope data was interpreted to demonstrate a hyperbolic trend, which the researchers argued ruled out a physical mixture of two dolomite phases. González et al. also argued against a physical mixture of dolomite and calcite contamination because all the samples were at least 90% pure dolomite or calcite, and the trend observed required more than 10% contamination. The presence of zoned dolomite, and dolomite rhombohedra with cloudy cores, provided additional support for dolomite formation in a mixing zone. Isla de Mona is an ideal setting to revisit the mixing-zone-dolomitization debate because isotopic resetting during burial heating, and fluid interactions with volcanics and volcaniclastics can be eliminated as possible explanations (e.g. Machel, 2000).

This research is significant because dolomitization can either create or destroy porosity in carbonate rocks resulting in formation or destruction of hydrocarbon

reservoirs (Sun, 1995). Dolomite reservoirs are estimated to contain 80% of the recoverable oil and gas reserves stored in carbonate rocks in North America (Davies, 1979). Reservoir quality in dolomites depends on several factors such as, original sedimentary fabric, formation mechanism, fracturing, karstification, burial compaction, and others (Sun, 1995). It is important to understand whether or not the mixing dolomitization model is valid, and to develop criteria that allow for identification of mixing-zone and other forms of dolomitization in the geologic record. The Isla de Mona carbonate platform is similar to subsurface carbonate reservoirs in Malaysia, Indonesia, and the Philippines (Wilson and Bosence, 1997; Kusumastuti et al., 2002; Neuhaus et al., 2004; Vahrenkamp et al., 2004) and can serve as an outcrop analog for porosity development in the subsurface.

Geologic Setting:

IM is a small island (55 km^2) that lies within the Mona Passage between Puerto Rico and the Dominican Republic (Figure 3). There are two formations exposed on the surface and coastal cliffs of the island; the Pliocene Lirio Limestone (LLS) and the underlying Miocene Isla de Mona Dolomite (Briggs and Seiders, 1972). The formations are separated by an island-wide unconformity. The Isla de Mona Dolomite was described as a thick to very thick, locally cross bedded, white, finely crystalline calcitic dolomite, whereas the Lirio Limestone was described as a thickly bedded, white to light yellow, finely crystalline limestone (Briggs and Seiders, 1972). Kaye (1959) originally named the Isla de Mona Dolomite as the Isla de Mona Limestone (IML) and described it as a "thick-bedded, dense, and finely crystalline limestone and dolomite that makes up most of Isla de Mona". Kaye hypothesized that the formations were separated by an erosional

unconformity. He assigned an age of early to middle Miocene to the IML, and a Pliocene age to the Lirio Limestone. Briggs and Seiders (1972) hypothesized plunging folds to be the cause of the observed geometries, and assigned a middle Miocene age to both formations. Further study by Rodríguez-Delgado (2012) confirmed that the limbs of the folds were actually clinoforms and that there is an island-wide erosional unconformity that supported Kaye's original interpretations and nomenclature; i.e. Lirio Limestone for the Pliocene to Pleistocene units above the island-wide unconformity, and Isla de Mona Limestone (IML) for the Miocene units below the unconformity. The Isla de Mona Dolomite, as described by Briggs and Seiders (1972), is mostly dolomite with beds of limestone below the contact with the LLS. Rodríguez-Delgado (2012) demonstrated that Briggs and Seiders (1972) failed to recognize the erosional unconformity separating the Miocene Limestone and the Pliocene to Pleistocene limestone. Rodriguez-Delgado suggested that neither the IML or Isla de Mona Dolomite names were adequate, as the IML descriptions failed to recognize the abundant dolomite present in the unit mapped as IML by Kaye (1959) and that Briggs and Seiders (1972) incorrectly placed the Miocene units below the erosional unconformity with the Pliocene-Pleistocene unit originally described by Kaye (1959). Rodriguez-Delgado suggested that the original IML unit be renamed Isla de Mona Formation and the limestone and dolomite portions of the Isla de Mona Formation be given member status. Given that it was determined to be more accurate, this research will use the nomenclature of Kaye (IML and LLS) rather than that of Briggs and Seiders.

The boundary between the IML and LLS as originally described by Briggs and Seiders (1972) is indeed a diagenetic boundary where a gradational transition from

dolostone to limestone occurs, as described by González et al. (1997). Rodriguez-Delgado noted that in some localities the LLS is dolomitized above the erosional contact and there is a sharp boundary (diagenetic) between the dolomitized LLS and the non-dolomitized LLS.

Strontium isotope ratios were obtained by González et al. (1997) and Adorno and Ramirez (2006) in order to date the dolomitization events. The values range from $0.708915 \pm 1.1x10^{-6}$ to $0.709041 \pm 6x10^{-6}$. These $^{87}Sr/^{86}Sr$ values indicate seawater ages from dolomite ranging from Serravallian to Zanclean (12.07 to 4.82 MA; Rodríguez-Delgado, 2012) based on the strontium curve and algorithms published in McArthur et al. (2001). Rodríguez-Delgado (2012) used biostratigraphy to date the Lirio Limestone and IML. Coral species within the IML correlate the formation to the Miocene. Above the unconformity, coral species place the age of the Lirio Limestone as Pliocene. Therefore, the dolomite formation could have been synchronous with deposition of the Pliocene units or could have taken place during both the Miocene and Pliocene. This agrees with the field evidence indicating dolomite formation occurring above the unconformity. One section measured by Rodríguez-Delgado (2012) found dolomite within the LLS, the Cueva Losetas lagoon section. The dolomite was present in the red algal wackestone facies above the unconformity, which is interpreted to represent a distal platform (platform interior) environment.

The IM carbonate platform records sea level fluctuations in the Caribbean. The IML was deposited during the Miocene in relatively shallow water and records a transgressive-regressive cycle, which ends in subaerial exposure and the formation of the island-wide unconformity. The platform experienced tilting in the Miocene prior to the

formation of the unconformity (i.e. it is an angular unconformity in places). Sea level rose during the Pliocene, and the Lirio Limestone was deposited over the unconformity. During the Middle Pleistocene, IM experienced three episodes of uplift to reach its current position, and tectonic activity caused additional tilting of the island to the southwest (Rodríguez-Delgado, 2012).

Fourteen facies were identified and interpreted by Rodríguez-Delgado (2012; Figure 4). The Massive coral framestone, and *Acropora*-rich framestone facies were interpreted to be patch reefs. A red algal wackestone facies was interpreted to be a distal platform environment (center of platform interior), whereas the skeletal packstone-grainstone, benthic foraminiferal grainstone, and red algal, molluscan, coral wackestone to packstone facies were all interpreted to be proximal platform (edge of platform interior). The massive coral framestone and coral floatstone facies were interpreted to represent the back reef environment. The reef crest was interpreted to include *Acropora* rich framestone, *Stylophora* rich framestone, and branching coral rudstone to floatstone. The interpreted forereef includes a *Meandrina* rich framestone, green algal wackestone to packstone, and branching coral rudstone to floatstone. Three facies were interpreted to represent the reef slope environment: large benthic and planktonic foraminiferal packstone to grainstone, green algal wackestone to packstone, and a branching coral rudstone to floatstone. Lastly, a planktonic foraminifera wackestone was interpreted as the open shelf environment. The interior of the island hosts patch reefs, distal platform, and proximal platform environments, and the reef core is located along the southeast and western edges of the island (Figure 5). Rodríguez-Delgado (2012) determined that dolomitization is restricted to the platform interior facies (proximal and distal platform),

which are also high in red algal grains (Figure 6). It is important to note however, that there are red algal rich facies that are not dolomitized, and the dolomite is found in other grains other than the red algae. Facies that were examined in this study included the red algal wackestone, skeletal packstone to grainstone, and the red algal, molluscan, coral wackestone to packstone facies (all of which were dolomitized) as defined by Rodríguez Delgado (2012).

Methods:

Samples for this study were obtained from existing collections from research conducted by previous workers. Three stratigraphic sections were utilized: Capitan Great section (CGS) and Punta Este (PE) measured by various workers and reported by Gonzalez et al. 1997, and Uvero (UVE) measured and sampled by Rodríguez-Delgado (2012; Figure 7). Existing thin section collections were utilized for the study. Thin sections were stained with alizarin red S and screened for dolomite content. Stratigraphic sections and analyzed sample locations are shown in Figure 8.

The selected thin sections were examined using transmitted light petrographic and cathodoluminescence (CL) microscopy. Conventional petrographic analysis was performed using an Olympus BX60 microscope and a Qimage QICAM digital camera. Dolomite was classified using the Sibley and Greg classification scheme (Sibley and Greg, 1987). CL analysis was performed using a Cambridge Image Technology LTD stage Clmk4 mounted on a Leitz SM-LUX-POL microscope. Images were captured with a Qimage QICAM digital camera under operating conditions of 15.6 KV accelerating voltage, at around 0.6 mA with a 2.8 sec exposure time. For this study, the terms bright, dull, and moderate are used to characterize luminescence. Bright refers to phases with

highly luminescent character, and dull describes phases with very low luminescence. Moderate refers to phases that have low luminescence, but are slightly more luminescent than dull phases.

Petrographic image analysis (PIA) to determine percent of dolomite versus calcite and porosity was performed on 14 thin sections using the JMicrovision software. The dolomite and porosity percentages were determined using point counting, because the thin sections did not contain enough color contrast to accurately determine percentages using object extraction. Eight representative fields of view (at 10x magnification) were analyzed for each stained thin section from Uvero (Li, 2013). Point counts were only done on Uvero thin sections because the thin sections for CGS and PE were not made using blue epoxy. At least 400 points were counted for each photomicrograph. The percent dolomite values were then compared to porosity percentages in order to detect patterns in dolomite distribution and its relationship to extant porosity.

For fluid inclusion analyses, doubly polished thin sections of 14 samples were prepared at the University of Kansas Rock Prep Lab. As the inclusions were formed at near surface temperatures, the sections were heated to 175°C in an oven for 8 hours. This stretched the inclusions to generate bubbles. Primary fluid inclusion assemblages (FIAs) were selected and analyzed on a Linkam THMS600 heating and cooling stage. The inclusions were frozen and the final melting temperature of ice (T_m ice) was correlated to the salinity of the diagenetic fluid using the seawater-salt model (Goldstein and Reynolds, 1994). The chips that had been used for fluid inclusion analysis were later stained with alizarin red S to confirm that there was no calcite present, and then powdered for $\delta^{18}O$ and $\delta^{13}C$ stable isotope analysis. Twenty-eight chips were analyzed,

but the data from 3 chips were lost during analysis. The powdered chips were reacted at 75°C in 100% H_3PO_4, in a Kiel IV System connected to the inlet of a ThermoFinnigan MAT 253 dual inlet ratio mass spectrometer (Suarez et al., 2009). Precision was monitored by NBS-18 and NBS-19 analysis and was better than 0.1‰ for both carbon and oxygen.

Results:

General aspects of petrography:

This study's petrography built upon previous work by Rodríguez-Delgado (2012). Emphasis is placed on post depositional diagenetic events. The data include important stages of micritization, dolomite precipitation, dissolution, calcite precipitation, calcitization, and silicification with the following generalized characteristics:

Micritization and micrite envelopes are present along the edges of many of the original grains. Micrite envelopes are in some instances the only remnant that survives later dissolution and allows identification of precursor original skeletal grains. Replacement dolomite is found as fabric destructive planar-E to planar-S rhombohedra, or finer grained mimetic dolomite (commonly replacing micrite and original high magnesium calcite (HMC) grains, such as red algae and foraminifera. The CL petrography shows several generations of luminescent and non-luminescent phases. There is one replacement phase, which displays a dull red luminescence. The dull red luminescent phase replaces the cores of rhombohedra and mimetically replaces some grains. The cores that have been replaced are cloudy in transmitted light. There are five cement phases: a dark red luminescent phase, three non-luminescent phases, a zoned CL phase, and a blue to light orange luminescent dolomicrite cement phase. The non-micritic

cement phases are isopachous, E-planar, and pore filling. The micritic phase is pore filling.

Three distinct dissolution events can be identified. The first event created moldic pores, mostly of corals and benthic foraminifera. Two late stage dissolution events created both moldic and vuggy pores, and their relative timing can be determined by the type and sequence of pore filling cements.

Two calcite phases were identified: a non-luminescent phase and a bright orange luminescent phase. The bright orange phase is rhombohedral to subhedral and isopachous, and it precipitates as cement mostly over dolomite crystals and thus inherits the shape of substrate. The non-luminescent phase is either neomorphic (after quartz), or filling intercrystalline porosity. One chalcedony phase was found, which had an isopachous fibrous morphology.

Paragenesis:

Based on cross cutting relationships, CL petrography, and sequence of cementation, sixteen paragenetic events were identified (Figure 9).

Event 1: Deposition. This event involves the deposition of original grains, the most abundant of which are red algae, echinoderm fragments, benthic foraminifera, corals, mollusks, bryozoans, and micrite. For more detailed information, see Rodríguez-Delgado (2012) Original grains underwent micritization on the sea floor and formed micritic envelopes. Although it was not observed in this study, Gonzalez et al. (1997) described an early (possibly syndepositional) non-luminescent isopachous fibrous calcite cement around skeletal grains interpreted as a marine cement.

Event 2: Early fabric selective dissolution. Some grains (corals and amphisteginid forams) were dissolved to create moldic pores. In some cases these moldic pores were filled with marine sediment. Thus, the dissolution is interpreted to be early and to have occurred while on the seafloor.

Event 3: Sediment fill. Moldic pores created in the previous stage are internally filled with dark micritic marine sediment (Figure 11). In cases where the sediments only partially fill the molds, they form geopetal structures. In some areas, the micrite is converted to microspar.

Event 4: Dolomite precipitation. This event consists of the precipitation of dolomite rhombohedra in pore spaces created during event 2 dissolution. It is non-luminescent, and is limpid in transmitted light. In some places, this phase has a patchy luminescence. This phase varies from planar-E to planar-S.

Event 5: Dolomitization and recrystallization of earlier dolomite. This dolomite phase replaces the microcrystalline grains, grains that were originally HMC, remaining micritic envelopes that survived early dissolution, and the cores of some dolomite rhombohedra. It has a patchy moderate red luminescence. The initial precipitation of dolomite in stage 4 was likely poorly ordered non-stoichiometric dolomite, and was preferentially replaced by this more ordered and stable dolomite phase. In some places event 5 dolomite mimetically replaces original grains (commonly red algal grains), but in other places only ghosts of original grain textures can be distinguished (Figure 10).

Event 6: Dissolution. Vuggy pores and moldic pores (most commonly of mollusk fragments) are created by dissolution. These pores only contain events 7, 8, or 9 cements. If these pores existed prior to the stage 7 dolomitization, they should contain earlier

phases within them. In a few cases, the phase 5 dolomite appears to be truncated by these pore spaces, which also places this stage in this order.

Event 7: Dolomite precipitation. This event involves the precipitation of a dull red luminescent dolomite cement phase. This phase is planar-E. In places, these cements overlie event 3 geopetal sediment fills. Although this dolomite cement is present in a variety of pores, it is commonly the first cement phase in event 6 pores. It is found rarely in UVE section, and is more prevalent in PE and CGS sections (Figure 10).

Event 8: Dolomite precipitation. Pore reducing non-luminescent dolomite that is found over the event 7 cement phase. This phase is non luminescent, and planar-E. (Figure 10).

Event 9: Dolomite precipitation. This final dolomite event shows a banded luminescence in CL, with alternating luminescent and non-luminescent bands. This dolomite is planar-E. The initial band in the series tends to be brighter than the following bands. The number of bands present ranges from three to nine, with the most common number being five. This phase only precipitates over the event 8 dolomite. This phase is only present in the deeper portions of the measured sections (Figure 12).

Event 10, 11, 12, or 13: Calcite precipitation and calcitization. A brightly orange luminescent calcite cement is precipitated over the event 9 banded dolomite. This event must occur after event 9, but its order is ambiguous in relation to the subsequent three events. It is more common in PE but is rarely found in UVE and CGS. Some grains that were originally HMC are interpreted to have recrystallized to calcite during this event, because they have the same bright orange luminescence as this cement.

Event 10, 11, 12, or 13: Quartz precipitation. Fibrous chalcedony is rarely precipitated into open pore spaces. The quartz has a bright red luminescence in CL. Timing of quartz precipitation is constrained by one occurrence where it is over event 9 dolomite. Since it was only found in two thin sections, its timing relative to the previous three events is not clear.

Event 10, 11, 12, 13: Fracturing. These fractures cross cut grains and cements, including the event 9 dolomite. The fracturing must have occurred after event 9, but its order in relation to the previous and next two events is not clear. Fractures are filled with micritic calcite, along with brecciated fragments of the host rock. The fractures are a maximum of 2 mm wide. Fractures are linear, continuous, brittle, and do not show any evidence of shear. There is no mineralization associated with the fractures, or on the grains within the fractures (Figure 13).

Event 11, 12, or 13: Micrite precipitation. Previously formed fractures and interparticle porosity are filled in with micrite. This event must have occurred after the formation of the fractures, but because the fracture timing is unknown, the timing of the micrite is also ambiguous. This micrite displays a light orange to blueish luminescence in CL. The orange luminescence is more common in CGS and PE, whereas the blue luminescence is more common in UVE. In some areas, it grades from blue along the outside edges of the pore, to orange in the middle of the pore, so it is interpreted to be a single event (Figure 13).

Event 14: Calcite replacement and cement precipitation. Non-luminescent calcite partially and mimetically replaces the quartz, and precipitates in intercrystalline porosity. Where it precipitates in intercrystalline porosity it is nonplanar and completely fills the

remaining pore space. Whether the replacement and precipitation occurred as a single event or as separate events is unclear, but based on CL character, this cement is interpreted to be a single event (Figure 14).

Event 15: Dolomite dissolution. Some parts of the dolomite have been leached out. In some places certain growth zones are leached out preferentially, resulting in moldic pores within dolomite crystals. In other crystals, the dissolution appears patchy. Dissolution may have been controlled by stoichiometric ordering, where less stoichiometric layers and growth zones were preferentially leached away. The timing of this event is uncertain and could have occurred earlier (post event 9 dolomite and before event 12 or later). The timing of this event is based on the fact that there are no cements (calcite or dolomite) filling the molds, and it appears that no other events (e.g. fracturing) affect the molds. Therefore, it is placed at the end of the paragenesis (Figure 12) Based on the available data, it is unclear if this event is the same dissolution event that formed the caves found throughout the island, or if they are separate events. Cave development was interpreted to occur at multiple points throughout the Pleistocene (Kaye, 1959; Briggs and Seiders, 1974; Gonzalez, et al., 1997) based on the different depths of the cave floors. The caves are developed in both the IML and the LLS, and in many cases, the caves extend from the LLS into the IML. Therefore, the cave development postdates the deposition of the LLS, but their relationship to the later calcite stages is not known.

Dolomite distribution:

Dolomite percentages range from 100% to 14% (Figure 8). The amount of dolomite present is variable, with samples containing 100% dolomite throughout the Miocene part

of the section and less abundant dolomite reported in the Pliocene (Figure 8; Figure 6). Dolomite is found only in the facies interpreted to be lagoon environments in both the Miocene, and in the one section where dolomite was found in the Pliocene. There is no correlation between dolomite percentage and extant porosity percentage (Figure 15). This agrees with the work performed by Rodríguez-Delgado (2012), which indicated that porosity is controlled by original lithology before dolomitization. She found that grainstones and rudstones had higher porosity than wackestones and floatstones. That study also found secondary controls on porosity were original mineralogy and proximity to karsting or the unconformity surface. It must be pointed out, however, that the data apply only to the extant porosity, which has been reduced by significant calcite cement that postdates the dolomite. A relationship may have existed between dolomite and porosity prior to the porosity reduction during calcite cementation. The late dissolution of dolomite also complicates this relationship, although it is less significant.

Fluid inclusions:

Fluid inclusions were measured in dolomite from 14 samples from the UVE, CGS, and PE sections. Only inclusions that were part of primary FIAs were measured since those inclusions would contain fluids that were present at the time of precipitation. The inclusions are located along growth zones, large in relation to crystal size, or oriented in the direction of crystal growth (Figure 16). Therefore, they are interpreted to be primary. The sampled fluid inclusions were found in stages 7 and 8 dolomite. T_m ice values range from -1.9 to -3.2 °C (Figure 17). These values correspond to salinities ranging from 35

ppt to 63 ppt seawater salt equivalent respectively. The mode is -2.1 °C, which is equivalent to a salinity of 39 ppt seawater salt equivalent.

sample	PE 5	PE 6	PE7	CGS 2	CGS 3	CGS 4	CGS 5	CGS 12	UVE 1	UVE 4	UVE 9	UVE 10	UVE 13	UVE 15
$T_m$ice	-2.4	-2.3	-2.6	-2	-2.1	-2.1	-2.1	-2.1	-2.2	-2.2	-2.1	-2.4	-2	-2.4
$T_m$ice	-2.9	-2.6		-2.1	-2.8	-2.1	-2	-2.2	-2.5	-2.5	-3.2	-2.1	-1.9	-2.2
$T_m$ice	-2.3			-2.1	-2		-2.4	-1.9		-3.2	-2.3			-2.5
$T_m$ice				-2.3							-2.4			

Table 1- List of samples and corresponding fluid inclusion $t_m$ice data values in °C.

Stable Isotopes:

The data presented in this study builds upon data from González et al. (1997; Figure 18). Isotope data from dolomitic components were previously interpreted to demonstrate a hyperbolic trend between the marine and fresh water end-members (supporting dolomitization by a mixture of two fluids). New data obtained in this analysis are similar to the previously published isotope data, but show less overall depletion than the González et al. data, and appear linear rather than hyperbolic in distribution. The carbon isotope values range from -1.52 ± 0.1‰ VPDB to 3.66 ± 0.1‰ VPDB, and oxygen values range from 1.32 ± 0.1‰ VPDB to 4.59 ± 0.1‰ VPDB (Table 1). The data display a positive linear covariance with an R^2 value of 0.9662 (Figure 18). Fluid inclusion salinity values do not show a correlation with the stable isotope values (Figure 19 and Figure 20).

Sample	$\delta\,^{13}C$ VPDB	$\delta^{13}C/^{12}C$ Std Dev	$\delta\,^{18}O$ VPDB	$\delta^{18}O/^{16}O$ Std Dev
CGS-12-1	3.45	0.04	4.48	0.02
CGS-2-2	3.29	0.04	4.17	0.04
CGS-3	2.87	0.02	4.21	0.06
CGS-4-2	2.97	0.02	4.33	0.02
CGS-4-3	2.86	0.03	4.09	0.04
CGS-4-4	3.19	0.03	4.49	0.03
CGS-5-1	3.05	0.02	4.28	0.04
CGS-5-2	2.95	0.03	4.10	0.04

CGS-5-3	3.04	0.03	3.95	0.11
PE-5	3.03	0.02	4.12	0.06
PE-6	2.89	0.02	3.69	0.02
PE-7	3.00	0.01	4.28	0.01
UVE-1-1	3.01	0.04	4.10	0.04
UVE-1-2	3.19	0.04	4.23	0.02
UVE-10-1	-0.93	0.04	1.59	0.06
UVE-10-2	1.82	0.02	3.43	0.04
UVE-10-3	1.65	0.04	3.08	0.05
UVE-13-1	-1.52	0.03	1.32	0.02
UVE-13-2	-1.10	0.01	1.60	0.02
UVE-13-3	1.94	0.03	3.38	0.04
UVE-15-1	3.21	0.01	4.02	0.05
UVE-15-2	2.99	0.02	3.68	0.03
UVE-4-1	3.41	0.04	4.33	0.06
UVE-4-2	2.96	0.02	3.97	0.06
UVE-9	3.66	0.01	4.59	0.02

Table 2- list of samples and corresponding $\delta^{13}C$ and $\delta^{18}O$ values with their respective standard deviations.

Discussion:

The three stratigraphic sections analyzed in this study demonstrate a paragenesis involving multiple stages of dissolution, dolomite and calcite precipitation. Early dissolution of aragonitic components created pore space that was subsequently reduced by multiple phases of dolomite cement. Some of the remaining original grains were replaced by dolomite and the early dolomite cements were recrystallized. CL character indicates that later dolomite phases were not recrystallized. The final events include precipitation of calcite in the remaining pore space. The work done by Rodriguez-Delgado (2012), concluded that the Isla de Mona reef complex formed in six stages. Stage one involved deposition of the IML. The next stage occurred when sea level fell and exposed the platform, creating the erosional unconformity that separates the IML from the Lirio Limestone. Sea level rose again during stage three to deposit the Lirio Limestone. The fourth stage was uplift of the island. Pleistocene terraces formed in the

fifth stage, and the sixth stage involved another relative sea level drop to the present day level. This stratigraphic framework can help guide the interpretation of the data.

Timing of some of the dolomite phases can be inferred based on the diagenetic history observed. Dissolution is commonly thought to be associated with meteoric diagenesis associated with relative sea level fall (Lincoln and Schlanger, 1987). Minerals that are relatively stable in the marine realm may be unstable in the freshwater phreatic and vadose zone, and will therefore dissolve. The interpreted stratigraphy indicates two major exposure events and the paragenesis shows two main dissolution events as well, events 6 and 15. It is likely that dolomite phases 4 and 5 precipitated prior to the fall in sea level that formed the unconformity between the Miocene and Pliocene rocks, whereas dolomite phases 7, 8, and 9 precipitated after it, during or after the Pliocene. The recrystallization observed in event 5 supports this interpretation, which could have been caused by a change from marine to fresh waters. Dolomite 4 is non-luminescent but also has a patchy character in places, so it is probably (although unknown from the available data) also recrystallized. The zoned dolomite cement was not sampled for fluid inclusion salinity values, but zoned CL character is often associated with alternating oxidizing and reducing fluids. Such a change is commonly found in environments with alternating marine and meteoric waters but is also known in waters without any alternation in salinity (Machel and Burton, 1991). The zoned character could be a result of secular variations in climate or microbial activity affecting redox in an aquifer just as easily as salinity variation. The zoned phase is followed by a return to calcite precipitation. Precipitation of calcite could indicate a change to fresh water, which lacks a source of magnesium required for dolomite formation. The calcite phases are followed by dissolution, which

supports its association with the second major sea level fall and exposure event after deposition of the Pliocene. In addition, there is one strontium isotopic data point that corresponds to a Pliocene age within the Miocene rock (Adorno and Ramirez, 2006). This means that at least some of the dolomite in Miocene strata was formed during the Pliocene, and therefore after the unconformity formation.

Dolomitization can increase or decrease porosity, depending on a variety of factors such as mineralogy, carbonate ion source, replacement texture, etc. (Mountjoy and Marquez, 1997). In this study of the dolomite of IM, the amount of dolomite present was not found to have a direct relationship to the amount of extant porosity. It is possible, however, that the large amount of late pore-filling calcite has obscured the relationship between dolomitization and porosity. The petrographic observations suggest that the amount of dolomite would not likely be positively correlated with the amount of porosity. Much of the dolomite observed was cement, and therefore had a negative impact on preservation of porosity. This may support what other researchers have found, which is that the main control on porosity is the depositional texture. Other controls were mineralogy and proximity to the exposure surface/karsting (Rodríguez-Delgado, 2012). The new observations made in this study suggest that calcite cementation plays a major role.

The fluid inclusion evidence presented here indicates that dolomite stages 7 and 8 of the IML were formed in the presence of evaporated mesohaline water and normal marine water. Since the earlier dolomite phases were not sampled by the fluid inclusion analysis, their origin cannot be determined. The four dolomitization models that were considered plausible were marine, mixing, biogenic, and reflux. The fluid inclusion data

demonstrate that the dolomite precipitated in waters with salinities ranging from normal marine (35 ppt) to mesohaline evaporated marine water (up to 63 ppt), with the majority of samples indicating some level of evaporative concentration. These data rule out a strictly marine origin for the dolomite, which would result in salinities near normal marine only.

The dolomite is associated with red algal-rich facies (red algal wackestone, skeletal packstone to grainstone, and the red algal, molluscan, coral wackestone to packstone facies), which is consistent with what would be expected for a dolomite of biogenic origin. If the dolomite originated from the red algae, one would expect salinities to mirror the preferred environment of growth for red algae (33-42 ppm). Some of the observed salinities fall outside of this range. Although the dolomite is associated with red algal rich facies, it is not found in all the red algal rich facies, and non-red algal grains are also dolomitized. In addition, the petrography indicates that most of the dolomite is secondary to the red algae grains and even forms cements. This rules out a biogenic origin, although it is likely that the red algae provided a magnesium source for later dolomite formation (Nash et al., 2011).

The final two interpretations (mixing or reflux) are both worth considering given the fluid inclusion, stable isotope and petrographic data. The isotope data display a linear trend between depleted and enriched values. This could indicate either formation in a mixing zone, or a physical mixture of two dolomite types. The classical mixing zone model of fresh and marine water end members is ruled out with the fluid inclusion data, because the data do not fall between 0 and 35 ppt salinity. Mixing of fresh and mesohaline end members is possible, but because there are no salinity values measured

below 35 ppm, mixing with fresh water is not supported. Lower salinity fluid inclusions potentially exist, but were not sampled, or it is possible that the dolomite that formed from the lower salinity fluids had no fluid inclusions. If the salinity variation observed in the fluid inclusions was due to mixing between fresh and mesohaline waters, then one might expect correlations between fluid inclusion salinity and both $\delta^{18}O$ and $\delta^{13}C$. Since no correlation has been observed, once again fluid mixing is not supported. Still, given the possibility that the isotopic data are dominated by physical mixtures with a recrystallized dolomite phase, and the bias in preservation of fluid inclusions in only certain growth zones, mixing zone, however unlikely, cannot be completely ruled out.

The petrographic data provide additional support for a physical mixture of two dolomites of different origin and further discredit the fluid mixing hypothesis. The dolomite formed in events 4 and 5 show petrographic evidence of having recrystallized. Event 5 was followed by dissolution. It is possible that the fluid responsible for dissolution was fresh water, which also recrystallized the event 4 and event 5 dolomite. Because this phase was not sampled during the fluid inclusion analysis, its origin cannot be determined conclusively. Based on the paragenesis, phases 4 and 5 are likely to predate the unconformity surface. These phases would probably have been exposed to fresh water during the sea level fall that resulted in the formation of the sub-Pliocene unconformity. If events 4 and 5 were then recrystallized in fresh water and events 7, 8, and 9 were formed in mesohaline water and seawater, a physical mixture of the two phases would result in the linear trend observed in the isotope data.

Considering the above information, precipitation from seawater and mesohaline reflux are the most likely explanations for the IML dolomite. Reflux can occur with only

slightly elevated salinities ranging from 37 to 42 ppt (Simms, 1984). The salinities determined here would be enough to create a density contrast and cause downward flow through the platform. PIA indicates high percentages of dolomite throughout the exposed interval at UVE, and field workers have reported that the dolomite reaches a thickness of up to 80 meters. The areal extent of a mixing zone is limited, and would require repeated sea level fluctuations to move the mixing zone in order to form extensive dolomite (Machel 2004). Only two large-scale cycles of sea level transgression and regression are observed on the platform. With mixing, one would not expect to see dolomite up to the top of the Miocene platform. The distribution of the dolomite is more consistent with what would be expected in a reflux system. Dolomite is present directly below the exposure surface and continues down throughout the exposed platform interior facies. The dolomite above the unconformity is found only in a small portion of the platform interior, which is what would be expected in a reflux situation. If the reflux did not take place consistently during Pliocene deposition, dolomite would only form in a small portion of the lagoon, where evaporation was occurring. Reduction of porosity through cement precipitation (overdolomitization) is associated with supersaturated refluxing brines (Machel, 2004), which is observed at IM. In addition, the barrier causing restriction (the reef core environment) is not dolomitized. The salinities found in this study were not high enough to precipitate gypsum (>120 ppt), but Melim and Scholle (2002) argued for reflux dolomite formation at salinities below gypsum saturations based on stratigraphic relationships in the Capitan Reef Complex. Melim and Scholle (2002) also determined that 2 MA was enough time for mesohaline reflux to dolomitize about 80% of the Capitan fore reef facies. Jones et al., (2000) modeled dolomitization on

Enewetak atoll and found that reflux could account for the observed dolomite, even with the impeding flow from geothermal circulation in the 5 MA available. Goldstein (1996) and Goldstein and Benison (1996) demonstrated that the Enewetak dolomite was the result of mesohaline reflux, where young fluids dolomitized older Eocene strata. In addition, reflux has been shown to be an effective method of dolomitization in cases where no shales or aquitards are present (Machel, 2004), as is the case in Isla de Mona.

The Isla de Mona platform was initially interpreted to be a case of mixing zone dolomitization. This more detailed study indicates that mixing of fresh and marine waters was not the likely driver for dolomite formation. Although isotope data show a trend between fresh and marine signatures, the additional information provided by fluid inclusion data refutes the mixing zone model. The mixing zone model is theoretically feasible, but this study seems to substantiate other studies that question the real world validity of the mixing zone model. Many of the areas in which dolomite was initially thought to be precipitated in the presence of a mixing zone failed to take into account recrystallization and its affect on isotope signatures (e.g. Land, 1991). This appears to be another such case, where the paragenetic history was not fully understood prior to interpretation of isotopic data. Reflux dolomite on the other hand, has been shown to occur in modern day settings (Deffeys et al., 1965). This study further confirms the validity of the reflux model to explain dolomite formation in certain circumstances.

At IM, the dolomite is restricted to the distal and proximal platform settings, which are equivalent to a platform interior lagoon rimmed by non-dolomitized reefal margins and forereef slopes. Despite later tilting and erosion, the observed geometries along the transition from the Miocene reef core to the lagoon show that the lagoon was

deeper than the reef (Figure 6). Present day geometries appear to show the Pliocene lagoon facies to be higher than the reef, but this is again due to tilting in the Pleistocene. Based on fossil assemblages, the platform interior facies were interpreted to be very shallow (less than 5 m deep in places; Rodríguez-Delgado, 2012), which would have increased evaporative concentation. The Great Bahama Bank has water depths that are generally around 5.5-7.3 m (3-4 fathoms) and has a consistently mesohaline water mass (salinities typically range from 40 to 42 ppt with a maximum around 46 ppt depending on season; Newell et al., 1959). Therefore, a combination of shallow water depths and the paleohigh created by the reef core led to a restricted environment, which allowed for evaporative concentration of seawater in the platform interior. This evaporated water was denser than the normal marine water and flowed through the limestone. The evaporated fluid would have been supersaturated with respect to dolomite. With the available data, it is impossible to determine the origin of dolomites 4 and 5, but based on the platform morphology, there was restriction present during the Miocene. Therefore, the same processes of reflux could have been occurring at that time to form dolomites 4 and 5. Later, perhaps when sea level fell before Pliocene deposition, and exposed the island, a fresh water lens developed and caused dissolution and recrystallization of the event 4 and event 5 dolomite. Currently only a small 10 m thick fresh water lens exists on the island (González et al., 1997), but during the 16th through 18th centuries the island was used as a watering port and had fresh water sources (Kaye, 1959). Kaye also interpreted the cave systems within the Lirio Limestone to have been formed by the presence of a perched water table. Although this occurred during the Pleistocene (and therefore after the formation of the dolomite) it demonstrates that during periods of low relative sea level,

fresh water lenses can develop within the platform. When sea level subsequently rose again, the restricted environment formed by the Pliocene reef led to reflux at times. This mesohaline fluid caused the precipitation of event 7 and 8 dolomites. When sea level fell and exposed the island again, precipitation of dolomite stopped and calcite precipitation and karsting (González et al., 1997) occurred.

Conclusions:

The Isla de Mona platform has been pervasively dolomitized during the Miocene to Pliocene epochs. The amount of dolomite present varies throughout the IML, but includes high percentages of dolomite near the top of the IML. Petrography demonstrates the existence of both recrystallized dolomite and dolomite that has not recrystallized. The recrystallized phase formed in unknown conditions and likely recrystallized in fresh water during an event of subaerial exposure separating the Miocene from the Pliocene. Later dolomite postdated that boundary and has fluid inclusion salinity values consistent with normal marine to slightly evaporated marine fluids. This salinity range and petrography eliminates a strictly marine origin for the dolomite, along with the biogenic formation model. Isotope data show a linear trend between enriched marine values and depleted fresh water values. This likely indicates a physical mixture of two dolomites, one that formed in marine and mesohaline waters and another that recrystallized in freshwater. Although mixing between evaporated marine and fresh water end members cannot be definitively disproven, this explanation is unlikely given the absence of fluid inclusion salinities below normal marine values. Therefore, the most likely explanation for the origin of much of the dolomite is from evaporated marine fluids. Sea level fall at

the end of the Miocene caused subaerial exposure and led to recrystallization of the early dolomite phases in meteoric water. After sea level rose in the Pliocene, the presence of reefal rims on the platform margin and shallow water depths created restriction. This led to evaporative concentration in the platform interior; the denser evaporated fluid would have refluxed downward, which induced the precipitation of the non-recrystallized dolomite. Additional fluid inclusion work focused on sampling the recrystallized dolomite phases would confirm the reflux origin and definitively exclude the mixing model.

References:

Adorno, Y., and Ramirez, W.R., 2006, Dolomitization in Mona Island: Department of Geology, The University of Puerto Rico, unpublished undergraduate thesis, under the supervision of Ramirez, W.R., Mayagüez, Puerto Rico, 37 pp.

Badiozamani, K., 1973, The dorag dolomitization model—application to the Middle Ordovician Wisconsin: Journal of sedimentary Petrology, v. 43, p. 965-984.

Briggs, R.P., Seiders, V.M., 1972. Geologic map of Isla de Mona quadrangle, Puerto Rico. U.S. Geological Survey Miscellaneous Investigation, Map 1-718.

Csoma, A.E., Goldstein, R.H. and Pomar, L., 2006, Pleistocene speleothems of Mallorca: implications for palaeoclimate and carbonate diagenesis in mixing zones: Sedimentology, v. 53, p. 213-236.

Csoma, A.E., Goldstein, R.H., Mindszenty, A. and Simone L., 2004, Diagenetic salinity cycles and sea level along a major unconformity, Monte Canposauro, Italy: Journal of Sedimentary Research, v. 74, p. 889-903.

Davies, G.R., 1979, Dolomite reservoir rocks: processes, controls, porosity development: American Association of Petroleum Geologists short course, 16 p.

Deffeys, K.S., Lucia, F.J., Weyl, P.K., 1965, Dolomitization of recent and Plio-Pleistocene sediments by marine evaporite waters on Bonair, Netherlands Antilles: Society of Economic Paleontologists and Mineralogists special publication v. 13, p. 71-88.

Gasworth, S.B., Budd, D.A., Farmer, G.L., 2007 The role and impact of freshwater—seawater mixing zones in the maturation of regional dolomite bodies within the proto Floridian Aquifer, USA: Sedimentology, v. 54, p. 1065-1091.

Goldstein, Robert H., 1996, Dolomite from Reflux of Moderate Salinity Brine, Enewetak Atoll: American Association of Petroleum Geologists Progs and Abstracts, p. A54.

Goldstein, R. H. and Benison, K.C., 1996, Cation, Anion and $^{87}Sr/^{86}Sr$ Analyses of Inclusion Fluids Elucidate Processes of Reflux Dolomitization, Enewetak Atoll: (extended abstract) Pan-American Conference on Research on Fluid inclusions, p. 48-50.

Goldstein, R.H., Reynolds, T.J., 1994, Systematics of fluid inclusions in diagenetic minerals: Society of Economic Paleontologists and Mineralogists short course, v. 31, 199 p.

González, L.A., Ruiz, H.M., Taggart, B.E., Budd, A.F., Monell, V., 1997, Geology of Isla de Mona, Puerto Rico, Developments in Sedimentology, v. 54, p. 327-358.

Hanshaw, B.B., Back, W., Deike, R.G., A geochemical hypothesis for dolomitization by ground water: Economic Geology, v. 66, p. 710-724.

Hardie, L.A., 1987, Dolomitization: A critical view of some current views: Journal of Sedimentary Petrology, v. 57, p. 166-183.

Jones, G., Whitaker, F., Smart, P., Sanford, W., 2000, Numerical modeling of geothermal and refluxcirculation in Enewetak Atoll: implications for dolomitization: Journal of Geochemical Exploration, v. 69-70, p. 71-75.

Kaufman, J., 1994, Numerical models of fluid flow in carbonate platforms: Implications for dolomitization: Journal of Sedimentary Research, v. 64, p. 128-139.

Krause, S., Liebetrau, V., Gorb, S., Sánchez-Román, M., McKenzie, J.A., Treude, T., 2012, Microbial nucleation of Mg-rich dolomite in exopolymeric substances under anoxic modern seawater salinity: new insight into an old enigma: Geology, v.40, p. 587-590.

Kaye, C.A., 1959, Geology of Isla Mona Puerto Rico, and notes on age of Mona Passage: Geological Survey Professional Paper.317c, 45 p.

Kusumastuti, A., Van Rensbergen, P., and Warren, J.K., 2002, Seismic sequence analysis and reservoir potential of drowned Miocene carbonate platforms in the Madure Strait, East Jave, Indonesia: American Association of Petroleum Geologists, v. 86, p. 213-232.

Land, L.S., 1973, Contemporaneous dolomitization of Middle Pleistocene reefs by meteoric water, North Jamaica: Bulletin of Marine Science, v. 23, p. 64-92.

Land, L.S., 1991, Dolomitization of the Hope Gate Formation (North Jamaica) by seawater; reassessment of mixing-zone dolomite: Geochemical Society Special Publication, v. 3, p. 121-133.

Li, Z., 2013, Diagenetic controls on porosity and permeability in Miocene carbonates, La Molata, Spain: Department of Geology, University of Kansas, Ph.D. thesis, Lawrence Kansas, 358 p.

Lincoln, J.M., Schlanger, S.O., 1987, Miocene sea-level falls related to the geologic history of Midway Atoll: Geology, v. 15, p. 454-457.

Luczaj, J.A., 2006, Evidence against the Dorag (mixing-zone) model for dolomitization along the Wisconsin Arch—A case for hydrothermal diagenesis: American Association of Petroleum Geologists Bulletin, v. 90, p. 1719-1738.

Machel, H.G., 2000, Dolomite formation in Caribbean islands—driven by plate tectonics?!, Journal of Sedimentary Research, v. 70, p. 977-984.

Machel, H.G., 2004, Concepts and models of dolomitization: a critical reappraisal, *in* Braithwaite, C.J.R., Rizzi, G. and Darke, G. eds., The geometry and petrogenesis of dolomite hydrocarbon reservoirs: Geological Society London Special Publication 235, p. 7-64.

Machel, H.G., and Burton, E.A., 1991, Factors governing cathodoluminescence in calcite and dolomite, and their implications for studies of carbonate diagenesis, *in* Barker C.E. and Kopp, O.C. eds., Luminescence microscopy and spectroscopy: qualitative and quantitative applications: Society of Economic Paleontologists and Mineralogists Short Course notes, p. 37-57

Machel, H.G., and Burton, E.A., 1994, Golden Grove Dolomite, Barbados; origin from modified seawater: Journal of Sedimentary Research, v. 64, p. 741-751.

Machel, H.G., and Mountjoy, E.W., 1986, Chemistry and environments of dolomitization; a reappraisal: Earth-Science Reviews, v. 23, p. 175-222.

Maliva, R.G., Missimer, T.M., Walker, C.W., Owosina, E.S., Dickson, J.A.D., Fallick, A.E., 2001, Carbonate diagenesis in a high transmissivity coastal aquifer, Biscayne Aquifer, southeastern Florida, USA: Sedimentary Geology, v. 143, p. 287-301.

Melim, L.A., Scholle, P.A., 2002, Dolomitization of the Capitan Formation forereef facies (Permian, West Texas and New Mexico): seepage reflux revisited: Sedimentology, v. 49, p. 1207-1227.

Melim, L.A., Westphal, H., Swart, P.K., Eberli, G.P., Minnecke, A., 2002, Questioning carbonate diagenetic paradigms: evidence from the Neogene of the Bahamas: Marine Geology, v. 185, p. 27-53.

Melim, L.A., Swart, P.K., Eberli, G.P., 2004, Mixing-Zone diagenesis in the subsurface of Florida and the Bahamas: Journal of Sedimentary Research, v. 74, p. 904-913.

Meyers, W.J., Lu, F.H., Zacariah, J.K., 1997, Dolomitization by mixed evaporative brines and freshwater, Upper Miocene carbonates, Nijar Spain: Journal of Sedimentary Research, v. 67, p. 898-912.

Morrow, D.W., 1982a, Dolomite-Part 1 The chemistry of dolomitization and dolomite precipitation: Geoscience Canada, v. 9, p. 5-13.

Morrow, D.W., 1982b, Dolomite-Part 2 dolomitization models and ancient dolostones: Geoscience Canada, v. 9, p. 95-107.

Mountjoy, E.W., Marquez, X.M., 1997, Predicting reservoir properties in dolomites: Upper Devonian Leduc buildups, deep Alberta basin *in* Kupecz, J.A., Gluyaz, J.,

Bloch, S., eds. Reservoir quality prediction in sandstones and carbonate, American Association of Petroleum Geologists Memoir 69, p. 267-306.

Nash, M.C., Troitzsch, U., Opdyke, B.N., Trafford, J.M., Russell, B.D., and Kline, D.I., 2011, First discovery of dolomite and magnesite in living coralline algae and its geobiological implications: Biogeosciences, v. 8, p. 3331-3340.

Neuhaus, D., Borgomano, J., Jauffred, J., Mercadier, C., Olotu, S., and Grotsch, J., 2004, Quantitative seismic reservoir characterization of an Oligocene Miocene carbonate buildup: Malapaya field, Philippines *in* Seismic imaging of carbonate reservoirs and systems: American Association of Petroleum Geologists, Memoir 81, p. 169-183.

Newell, N. D., Imbrie, J., Purdy, E. G., and Thurber, D. T., 1959, Organism communities and bottom facies, Great Bahama Bank: American Museum of Natural History Bulletin, v. 117, p. 181-228.

Price, R.M., and Herman, J.S., 1991, Geochemical investigation of salt-water intrusion into a coastal carbonate aquifer: Mallorca, Spain: Geological Society of America Bulletin, v. 103, p. 1270-1279.

Rodríguez-Delgado, A.M., 2012, Sedimentology and stratigraphy of the Miocene to Pliocene: Department of Geology, University of Kansas, M.S. thesis, Lawrence Kansas, 214 p.

Scholle, P.A., Ulmer-Scholle, D.S., 2003, A color guide to the petrography of carbonate rocks: Tulsa, American Association of Petroleum Geologists, 474 p.

Sibley, D.F., Gregg, J.M., 1987, Classification of dolomite rock textures: Journal of Sedimentary Petrology, v. 57, p. 967-975.

Smart, P.L., Dawans, J.M., Whitaker, F., 1988, Carbonate dissolution in a modern mixing zone: Nature, v. 335, p. 811-813.

Suarez, M.B., González, L.A., Ludvigson, G.A., Vega, J., Alvarado-Ortega, J., 2009, Isotopic composition of low-latitude paleoprecipitation during the Early Cretaceous: Geological Society of America Bulletin, v. 121, p. 1584-1595.

Tucker M., and Wright P., 1990, Carbonate depositional systems; I, Marine shallow-water and lacustrine carbonates (in Carbonate sedimentology) Blackwell Science, Oxford.

Vahrenkamp, V.C., David, F., Duijndam, P., Newall, M., and Crevello, P., 2004, Growth architecture, faulting, and karstification of a Middle Miocene carbonate platforms, Luconia province, offshore Sarawak, Malaysia: Seismic imaging of carbonate reservoirs and systems: American Association of Petroleum Geologist, Memoir 81, p. 329-350.

Vasconcelos, C., McKenzie, J.A., 1997, Microbial mediation of modern dolomite precipitation and diagenesis under anoxic conditions (Lagoa Vermelha, Rio De Janeiro, Brazil): Journal of Sedimentary Research, v. 67, p. 378-390.

Wilson, M.E.J., and Bosence, D.W.J., 1997, Platform-top and ramp deposits of the Tonasa carbonate platform, Sulawesi, Indonesia: Petroleum geology of Southeast Asia, Geological Society of America special publications, no. 126, p. 247-279.

Qing Sun, S., 1995, Dolomite reservoirs: porosity evolution and reservoir characteristics: American Association of Petroleum Geologists Bulletin v. 79, p. 186-204.

Figures:

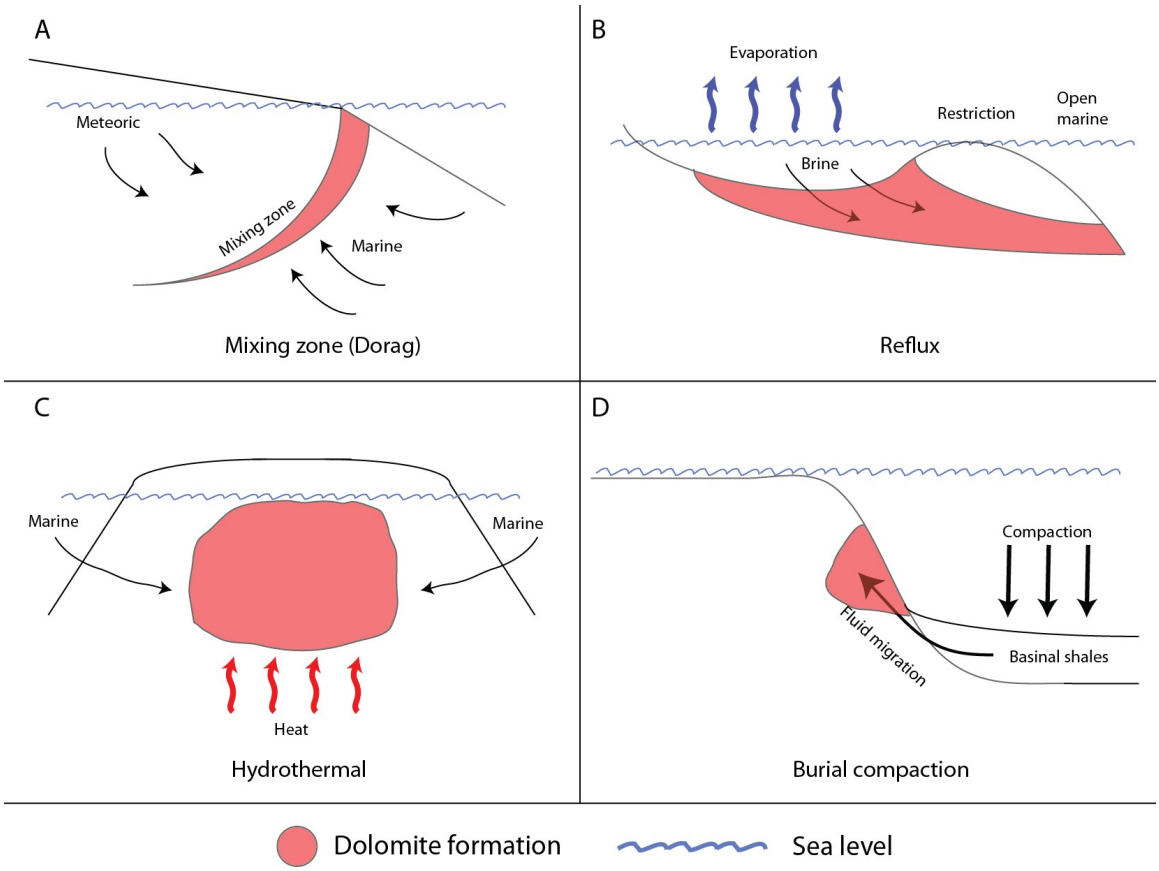

Figure 1: Representative cross sections of major dolomitization models. Arrows indicate direction of flow. A) Mixing of fresh and marine waters causes dolomitization along a zone of mixing. B) Evaporation in restricted locations causes the formation of dense brines, which sink and interact with nearby carbonate bodies. C) Hydrothermal fluids interact with carbonate bodies. D) Compaction of a basin-filling shale releases pore fluid into surrounding carbonate bodies.

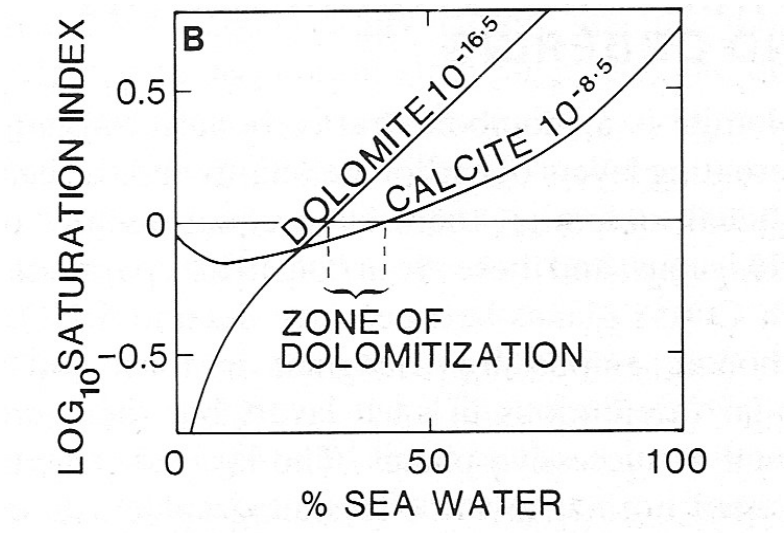

Figure 2: Graph of saturation index versus percent seawater.
Notice how a mixture of marine and fresh water can be undersaturated with respect to dolomite but saturated with respect to calcite (Tucker and Wright, 1990).

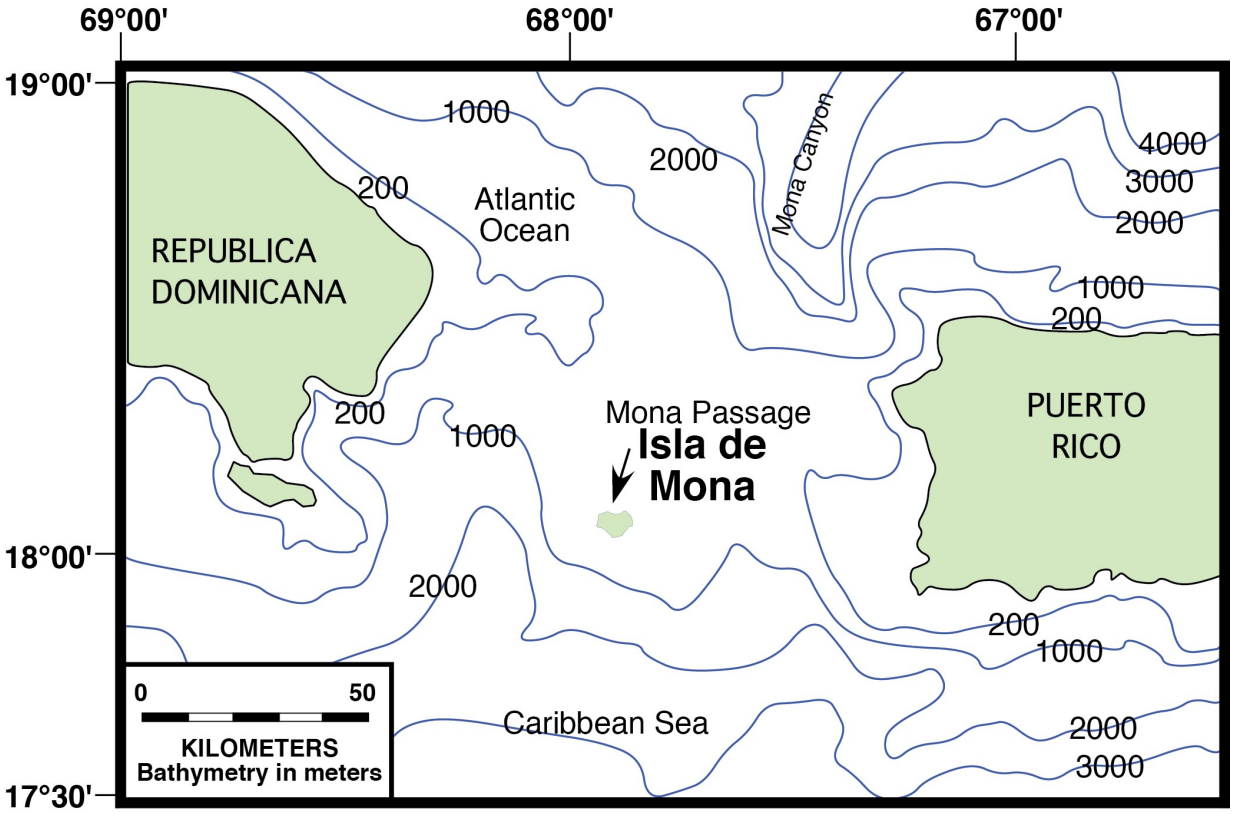

Figure 3: Location map of Isla de Mona and the Mona Passage.
Contours represent the bathymetry of the Mona Passage, with a contour interval of 1,000 meters (Modified from Kaye, 1959).

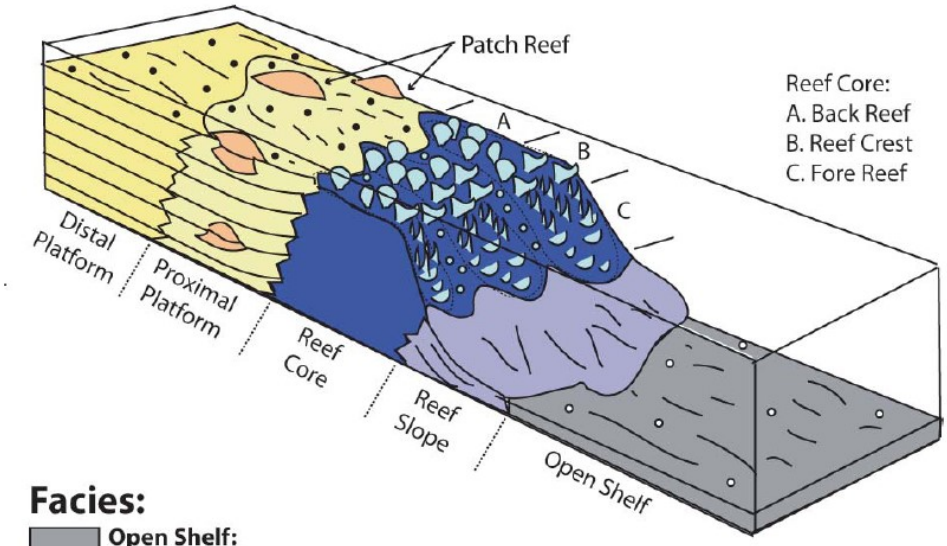

Facies:

Open Shelf:
(F13) Pelagic foraminifera wackestone

Reef Slope:
(F9) Large benthic and pelagic foraminifera packstone to grainstone
(F11) Green algae wackestone to packstone
(F12) Branching coral rudstone to floatstone

Reef Core; A. Back reef:
(F5) Massive coral framestone
(F6) Coral floatstone

Reef Core; B. Reef Crest:
(F7) *Acropora*-rich framestone
(F8) *Stylophora*-rich framestone
(F12) Branching coral rudstone to floatstone ?

Reef Core; C. Fore Reef:
(F10) *Meandrina*-rich framestone
(F11) Green algae wackestone to packstone
(F12) Branching coral rudstone to floatstone

Proximal Platform:
(F2) Skeletal packstone to grainstone
(F3) Benthic foraminiferal grainstone
(F4) Red algae, molluscan, coral wackestone to packstone

Distal Platform:
(F1) Red algae wackestone

Patch Reef:
(F5) Massive coral framestone
(F7) *Acropora*-rich framestone

Figure 4: List of facies and interpreted depositional environments.
Facies are as defined by Rodríguez-Delgado. The facies that were examined in this study are noted in red (modified from Rodríguez-Delgado, 2012).

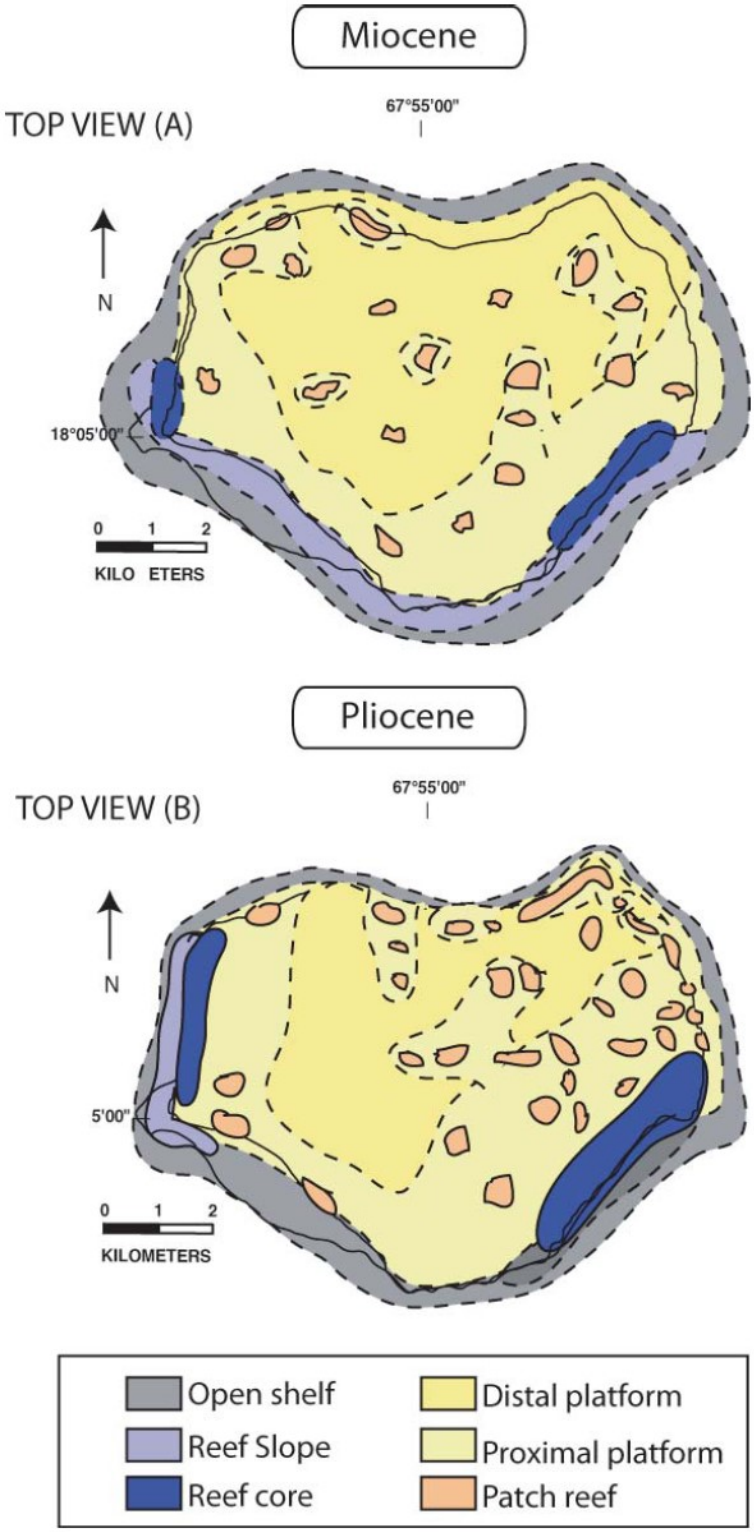

Figure 5: Map showing the distribution of environments on Isla de Mona.
The top (A) shows the distribution during the Miocene (IML) and bottom (B) shows the distribution during the Pliocene (LLS) periods (from Rodríguez-Delgado, 2012).

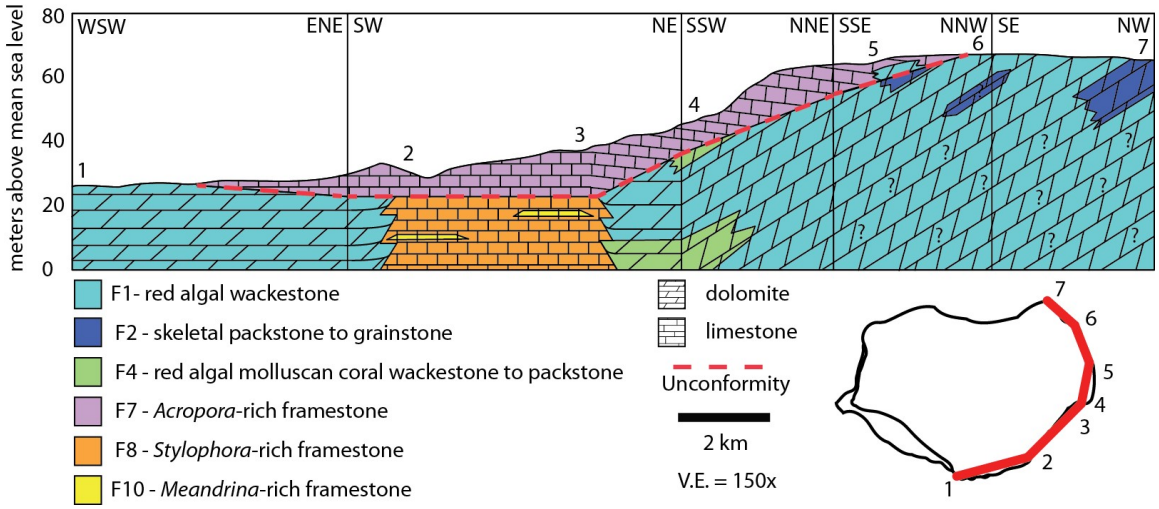

Figure 6: Cross section showing distribution of the dolomite along the cliffs of IM.
This figure shows the distribution of the dolomite within the IML and LLS. The platform interior environment is dolomitized, but the reef core is still limestone. The Lirio Limestone is present above the unconformity, and the IML is present below the unconformity. One measured section was dolomitized within the LLS (5), and was interpreted to represent a lagoon environment. The black vertical divisions indicate rotation of the cross section direction. The numbers indicate approximate location of sections measured by Rodríguez-Delgado (2012) as follows: Uvero (1), Playa de Pajaros (2), Cueva Escalera (3), Punta Este (4), Este reef and lagoon (5), Cueva Frio (6), and Cabo Norte (7). Refer to figure 7 for more detailed locations. Tilting to the southeast occurred prior to deposition of the LLS. Bedding from Uvero to Cueva Escalera is tilted, but due to the perspective of the cross section, they appear horizontal. Additional tilting to the southwest occurred during uplift of the platform during the Pleistocene. For more detailed information, see Rodríguez-Delgado (2012).

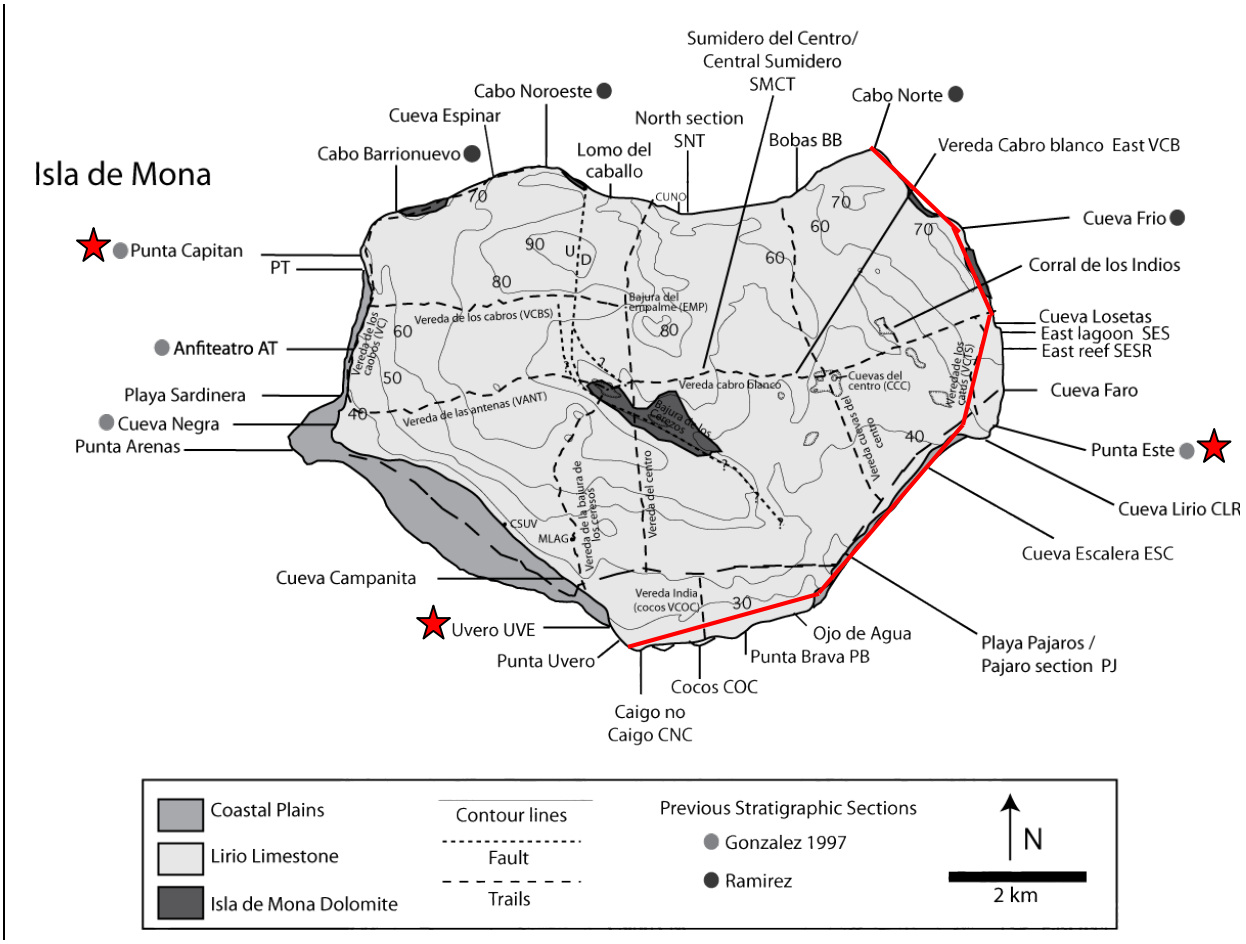

Figure 7: Geologic map of Isla de Mona showing locations of measured sections. The Isla De Mona Limestone is also exposed along the cliff faces. Red line indicates location of cross section for figure 6. Sections from which samples were analyzed in this study are noted with a star (modified from Rodríguez-Delgado, 2012).

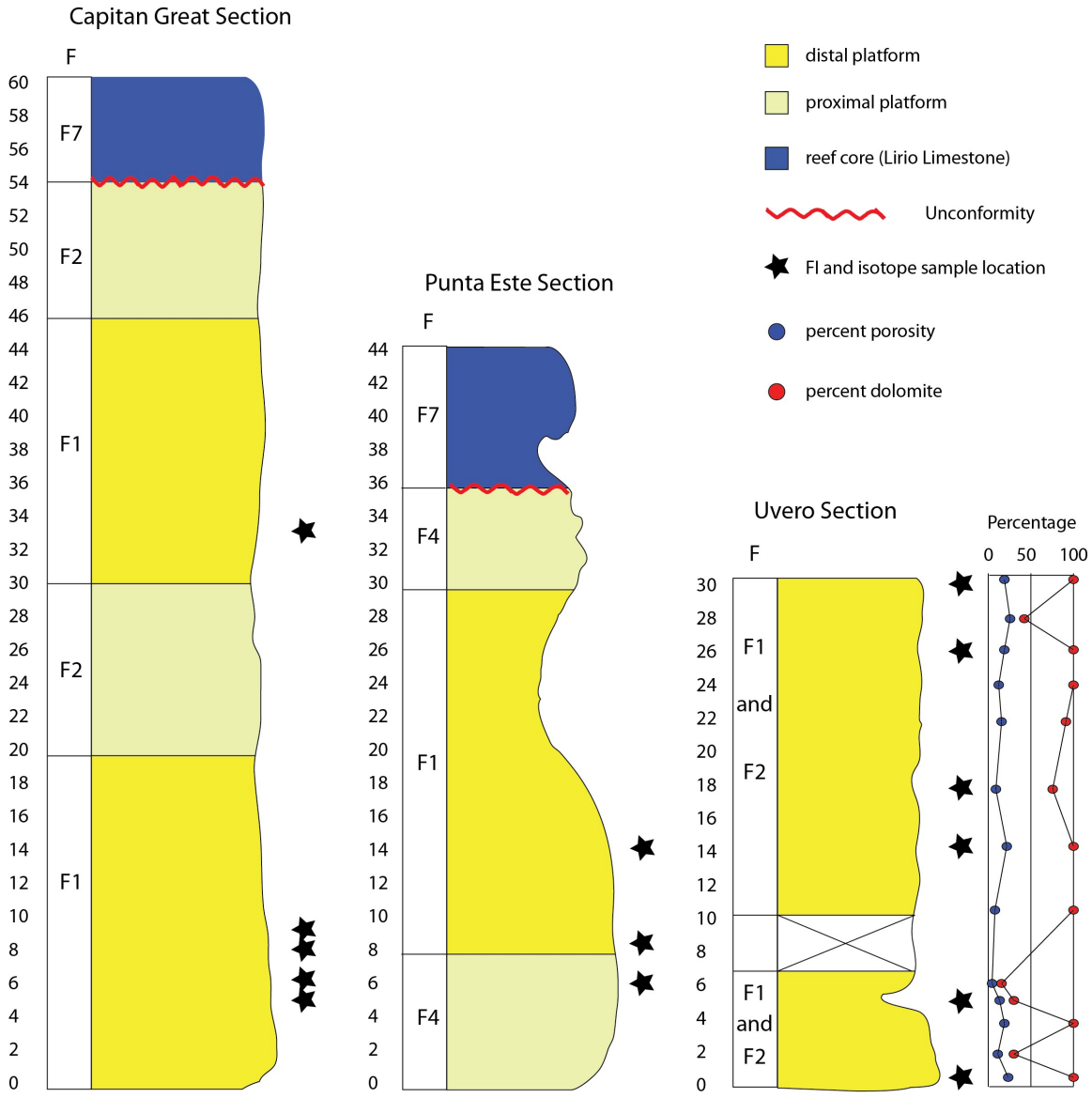

Figure 8: Stratigraphic columns for the measured sections analyzed. Columns show the interpreted environment of deposition, facies (column F; Rodríguez-Delgado et al., 2012), PIA analysis percentages, and locations for samples with measured fluid inclusions and stable isotope values. The depth scale is in meters. See fig. 4 for facies key.

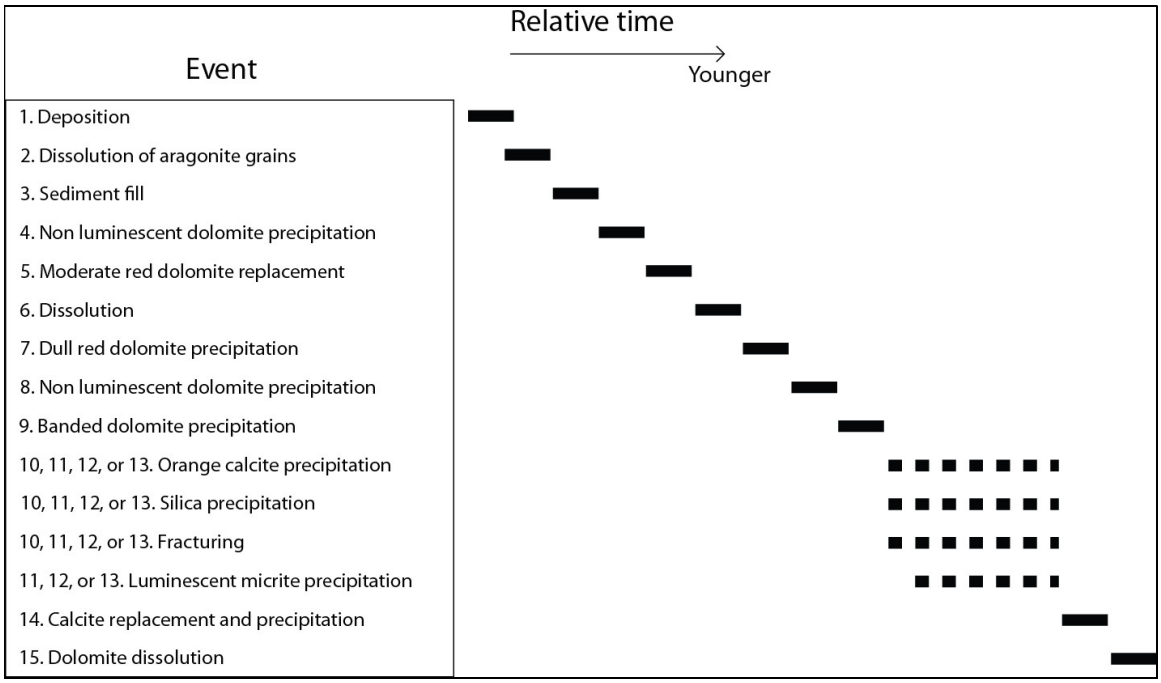

Figure 9: List and relative timing of paragenetic events.
Dashed lines indicate uncertain timing.

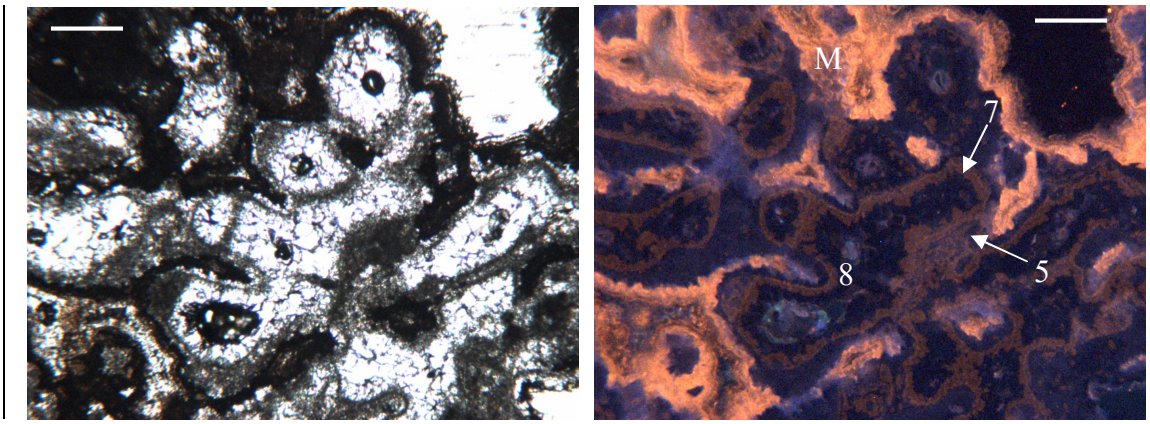

Figure 10: Transmitted light and CL image from sample PE-2.
Diagenetic events are numbered. Note the micritic envelope formed along the outside of the coral grain. M denotes the micrite phase that is placed at either event 10, 11, 12, or 13. Scale bar is about 250 microns.

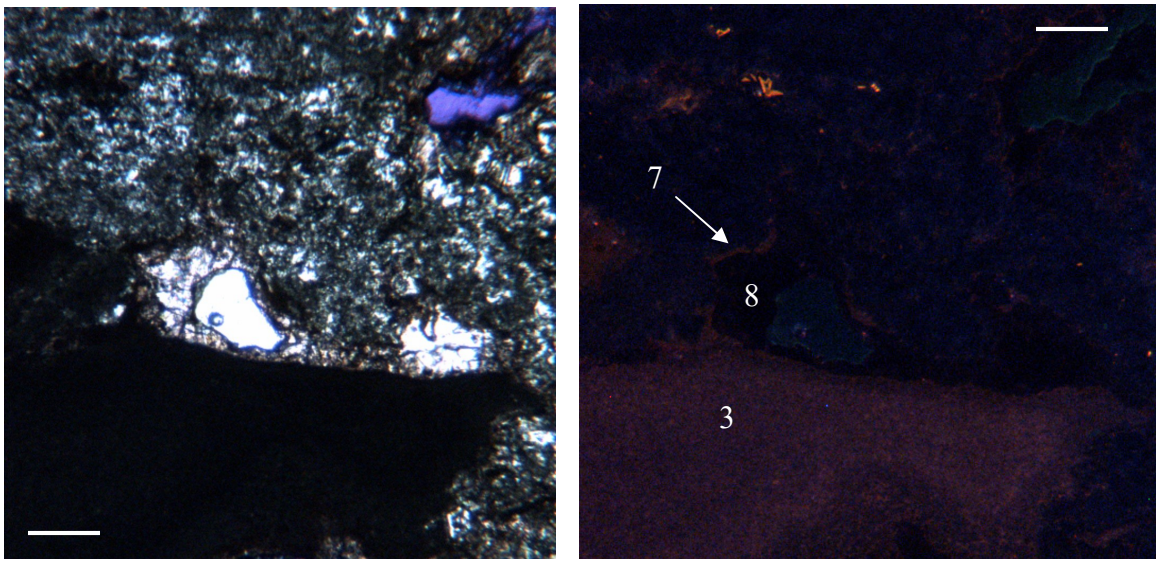

Figure 11: Transmitted light and CL image of sample CGS-4
Figure shows an event 3 geopetal fill lined with event 7 and 8 dolomite cements. Scale bar is about 250 microns. Image has been enhanced by adjusting brightness and contrast to better illustrate the luminescence of this sample.

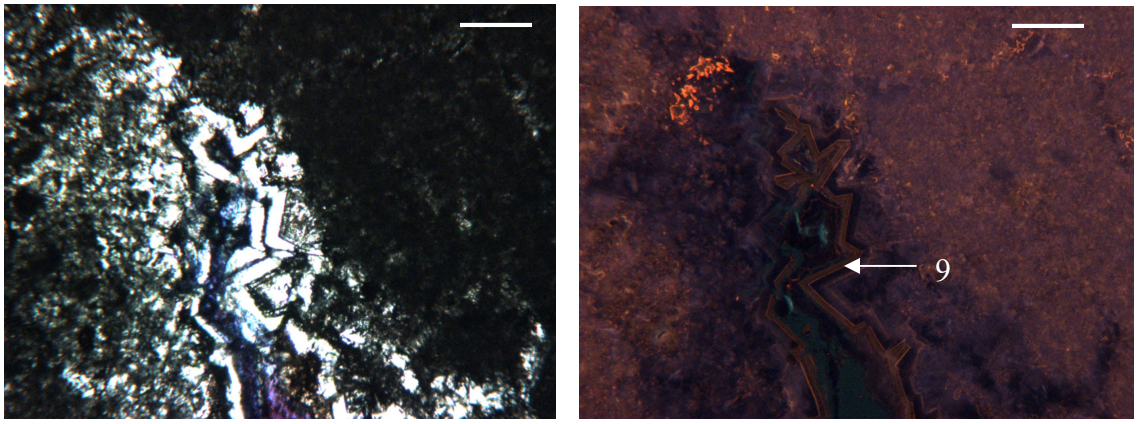

Figure 12: Transmitted light and CL image of a sample from UVE-3.
Figure shows the event 9 zoned dolomite cement, along with dolomite leaching. Scale bar is about 250 microns.

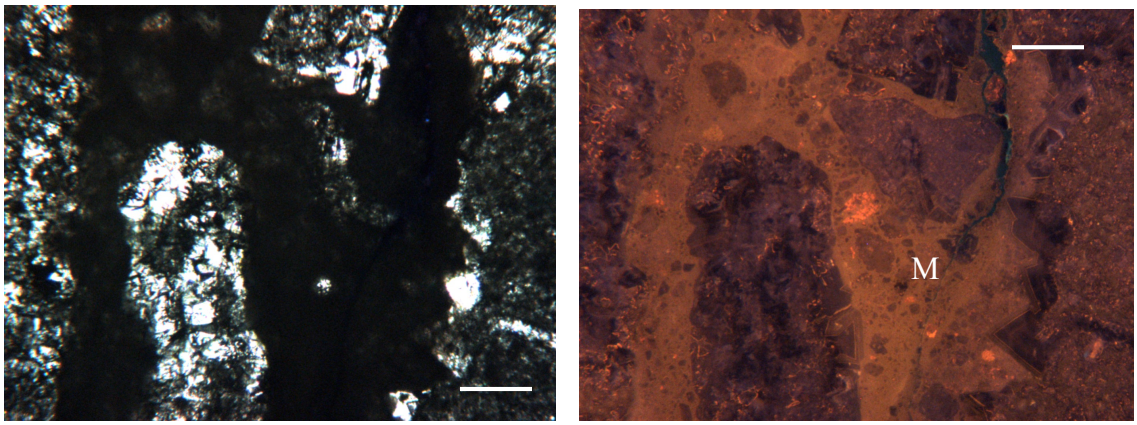

Figure 13: Transmitted light and CL image of a sample from UVE-3.
Figure shows an event 10, 11, 12, or 13 fracture filled with micrite and brecciated fragments of the host rock. It is likely a karst feature. Note the event 9 banded dolomite rhombohedra are cross cut by the micrite fill indicating fracturing. Scale bar is about 250 microns.

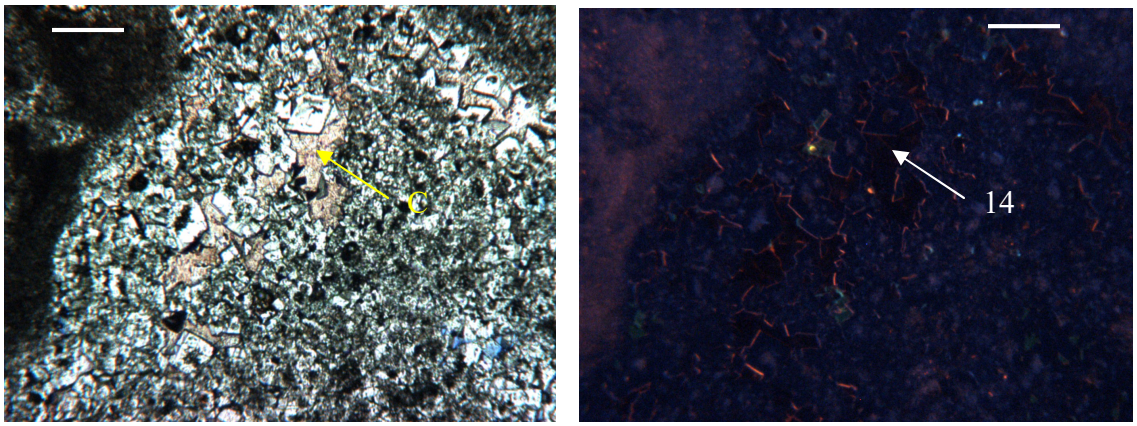

Figure 14: Transmitted light and CL image of a sample from UVE-1.
Figure shows the event 14 pore filling non luminescent calcite (C) (stained light pink in transmitted light). Scale bar is about 250 microns. Image has been enhanced by adjusting brightness and contrast to better illustrate the luminescence of this sample.

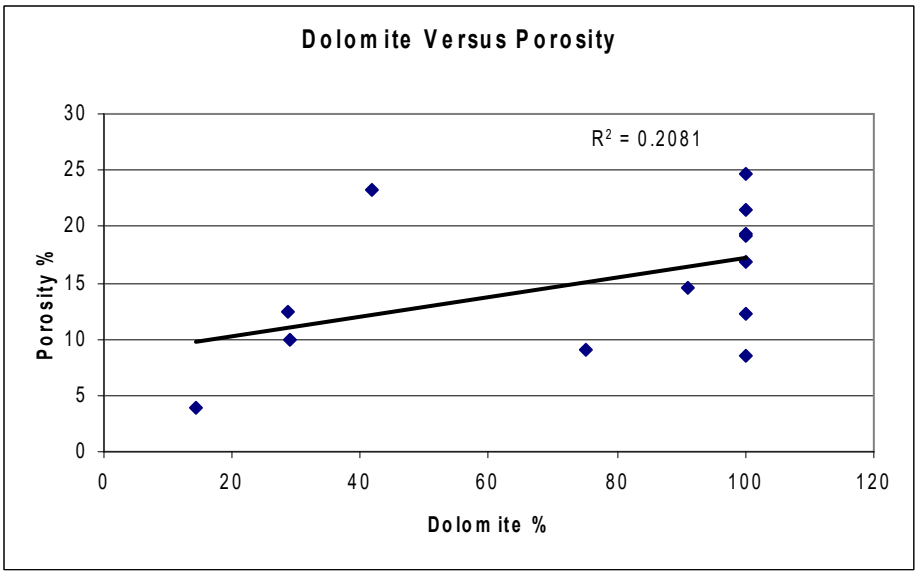

Figure 15: Graph of percent dolomite versus percent extant porosity. No trend is present.

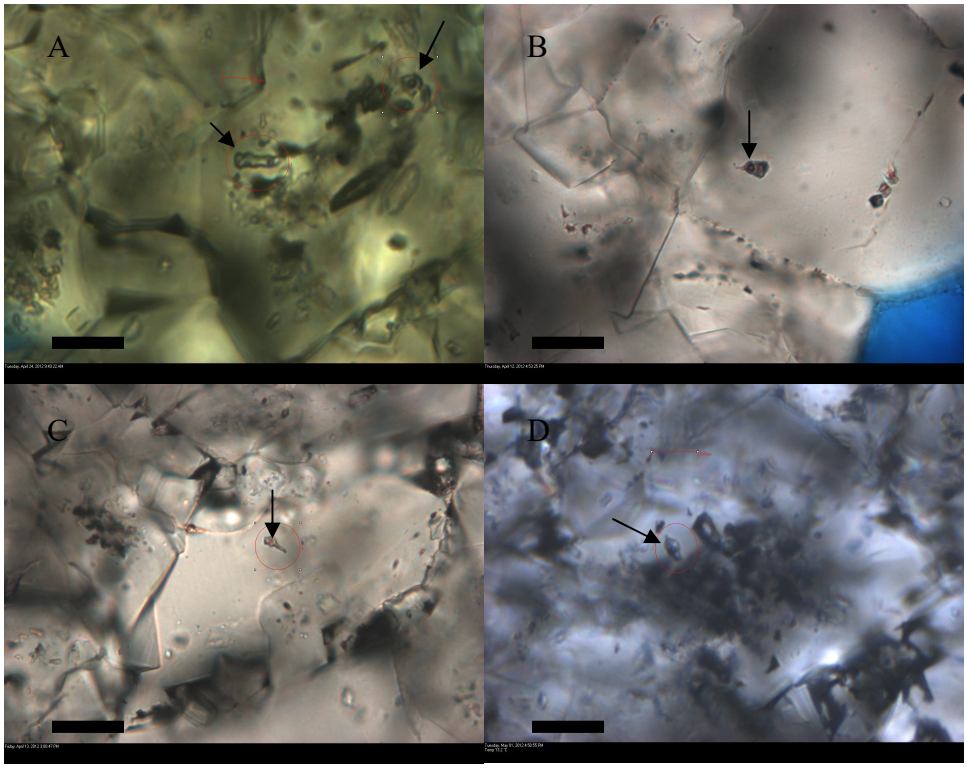

Figure 16: Photomicrographs of fluid inclusions.
Scale bar is 10 microns. Arrows indicate fluid inclusions. Fluid inclusions are interpreted to be primary in origin. A) Two fluid inclusions along a growth zone. B) Fluid inclusion that is elongated in growth direction. C) Fluid inclusion that is elongated in growth direction. D) Fluid inclusion that is elongated in growth direction.

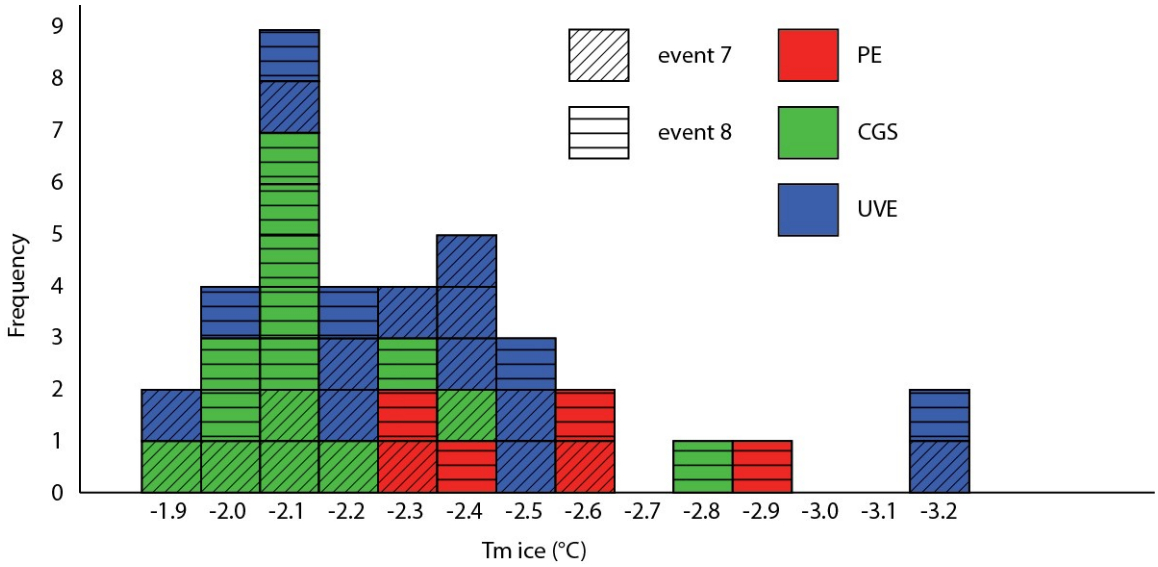

Figure 17: Histogram of fluid inclusion data.
The graph shows the frequency and distribution of each T_m ice value for each measured fluid inclusion, color-coded by sample location.

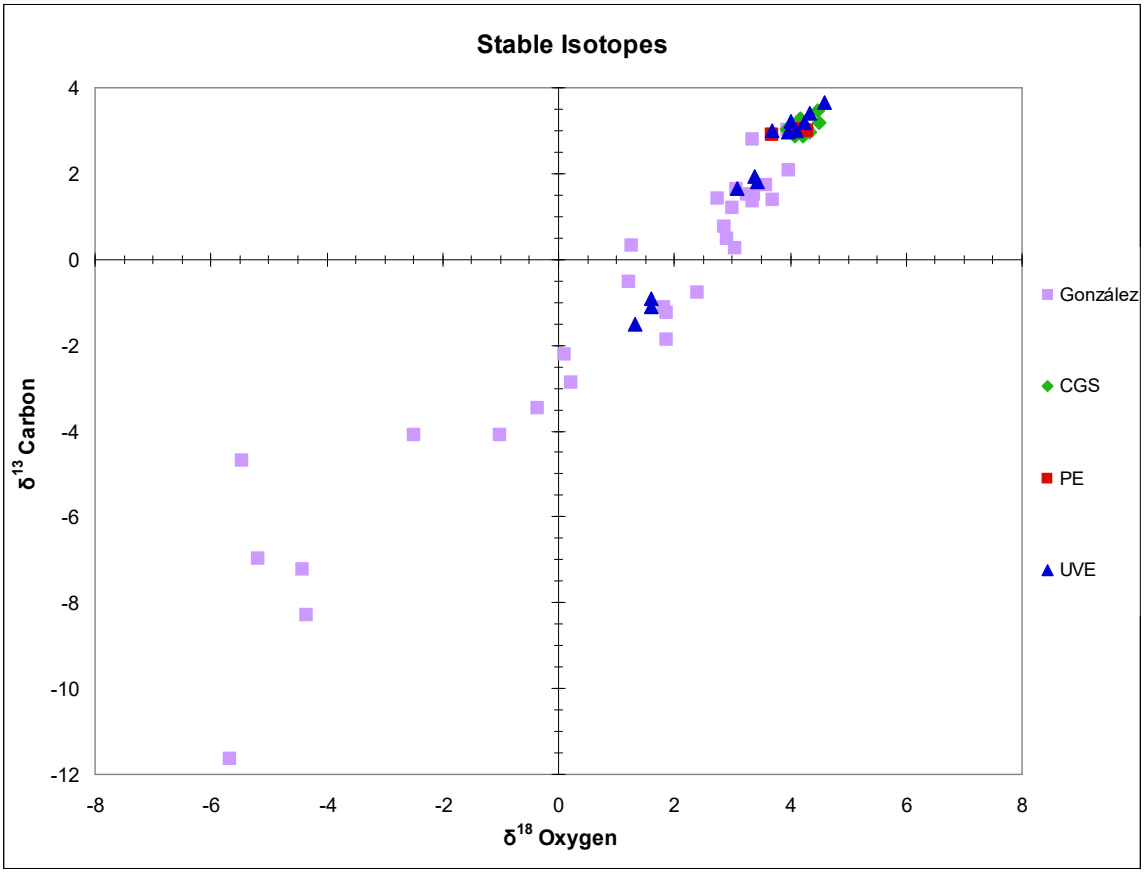

Figure 18: Crossplot of stable isotope data.
Figure includes the stable isotope data analyzed for this study, and data from the dolomitic components analyzed by González (1997). Samples are separated by the three measured sections that were sampled. The data show a linear trend with positive covariation.

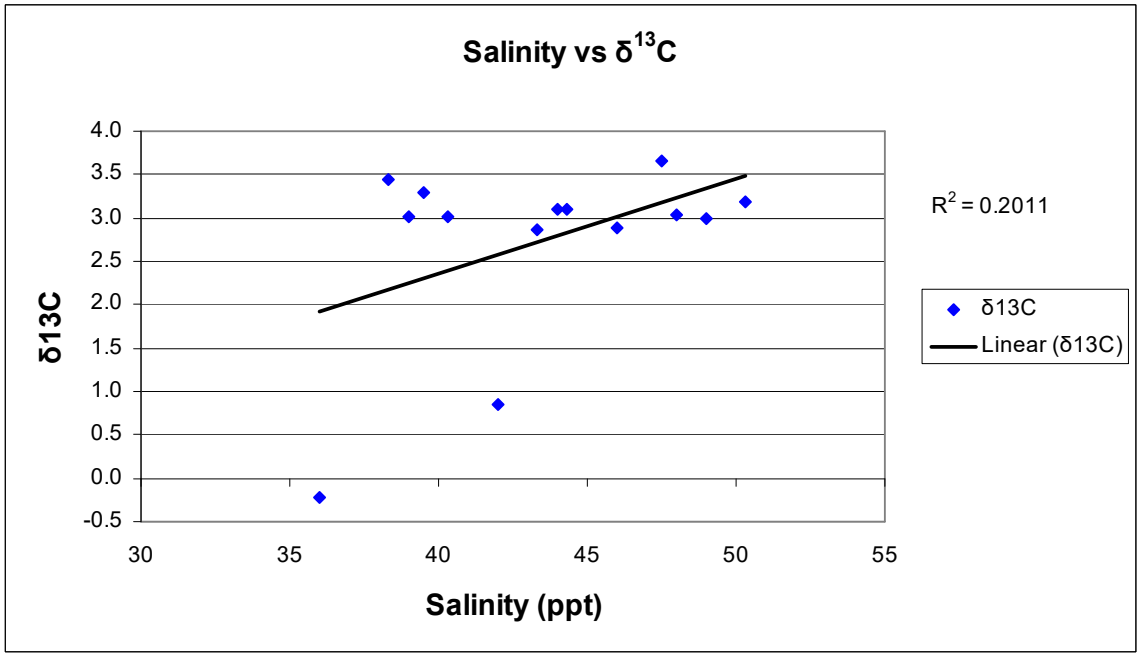

Figure 19: Graph of average fluid inclusion salinity versus δ ^{13}C.
There is no trend present.

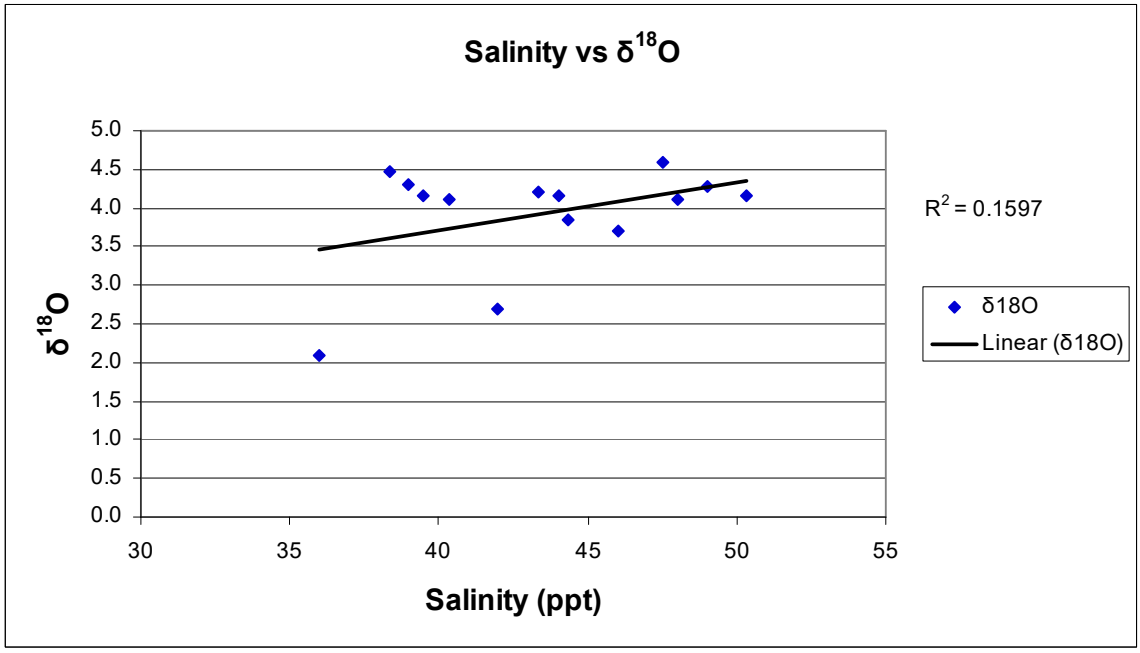

Figure 20: Graph of average salinity versus δ ^{18}O.
There is no trend present.